

Deformation in western Guatemala associated with the NAFCA (North America-Forearc-Caribbean) triple junction: Neotectonic strain localization into the Guatemala City graben

Bridget Garnier¹, Basil Tikoff¹, Omar Flores², Brian R. Jicha³, Charles Demets¹, Beatriz Cosenza Muralles¹, Walter Hernández⁴, and David C. Greene⁵

¹University of Wisconsin-Madison

²USAC

³Department of Geoscience, University of Wisconsin-Madison

⁴Observatorio Ambiental, Ministerio de Medio Ambiente y Recursos Naturales (MARN)

⁵Denison University

November 26, 2022

Abstract

Recent structural and geodetic data define the Guatemala City graben region as the continental triple junction between the North American plate, Caribbean plate, and a forearc sliver. We present a minor fault analysis, geochronological and geochemical analyses, and newly updated GPS velocities in western Guatemala, west of the Guatemala City graben, to characterize the magnitude and timing of extensional deformation in this poorly understood area. Elongations estimated from fault data are parallel (east-west) and perpendicular to the Polochic-Motagua fault system to the north, similar to geodetically-measured active deformation observed east of the Guatemala City graben. Four new $^{40}\text{Ar}/^{39}\text{Ar}$ dates and correlation of tephra deposits suggests that faulting was active during the Pliocene, but ceased eastward towards the Guatemala City graben over time. From west to east, fault cessation occurred before the deposition of the Los Chocoyos ash (84 ka) and E tephra (51 ka). Faulting just west of the Guatemala City graben appears to be active, where a major fault cuts the most recent Amatitlan tephra. Based on this data, we propose a time-progressive strain model for deformation related to North America-Caribbean plate interactions, whereby distributed elongation of the westernmost Caribbean plate occurred during the Pliocene but localized mostly within the Guatemala City graben and nearby faults during the Quaternary. Our model supports that: 1) The Guatemala City graben is effectively the western limit of the Caribbean plate; and 2) Western Guatemala, which used to be the trailing edge of the Caribbean plate, has been transferred to the forearc region.

Hosted file

appendix_preprint.docx available at <https://authorea.com/users/554297/articles/605562-deformation-in-western-guatemala-associated-with-the-nafca-north-america-forearc-caribbean-triple-junction-neotectonic-strain-localization-into-the-guatemala-city-graben>

1 **Deformation in western Guatemala associated with the NAFCA (North**
2 **America-Forearc-Caribbean) triple junction: Neotectonic strain localization**
3 **into the Guatemala City graben**

4
5 **Bridget Garnier¹, Basil Tikoff¹, Omar Flores², Brian Jicha¹, Charles DeMets¹, Beatriz**
6 **Cosenza-Murales^{1,3}, Walter Hernandez⁴, David Greene⁵**

7 ¹University of Wisconsin-Madison, Department of Geoscience, 1215 West Dayton St., Madison,
8 WI 53706

9 ²Centro de Estudios Superiores de Energía y Minas, Edificio T-1, Universidad de San Carlos de
10 Guatemala, Ciudad Universitaria, Zona 12, Guatemala, Guatemala 01012

11 ³Instituto de Investigación en Ciencias Físicas y Matemáticas, Escuela de Ciencias Físicas y
12 Matemáticas, Universidad de San Carlos de Guatemala, Ciudad Universitaria, Zona 12
13 Guatemala, Guatemala 01012

14 ⁴Ministerio de Medio Ambiente y Recursos Naturales, Km. 5 1/2 carretera a Santa Tecla, colonia
15 y calle Las Mercedes, San Salvador, El Salvador

16 ⁵Denison University, Olin Science Hall, 100 Sunset Hill Rd., Granville, OH, 43023

17

18 Corresponding author: Bridget Garnier (bridget.garnier@me.com)

19

20 **Key Points:**

- 21 • The Guatemala City graben region is the current North America, Forearc, and Caribbean
22 plate triple junction.
- 23 • Faulting in western Guatemala, representing internal deformation of the Caribbean plate,
24 ceased in an eastward fashion over the past ~4 Ma.

- 25 • Distributed deformation once extended across Guatemala and into Honduras and has
26 localized into the Guatemala City graben region over time.

27 **Abstract**

28 Recent structural and geodetic data define the Guatemala City graben region as the
29 continental triple junction between the North American plate, Caribbean plate, and a forearc
30 sliver. We present a minor fault analysis, geochronological and geochemical analyses, and
31 newly updated GPS velocities in western Guatemala, west of the Guatemala City graben, to
32 characterize the magnitude and timing of extensional deformation in this poorly understood area.
33 Elongations estimated from fault data are parallel (~east-west) and perpendicular to the Polochic-
34 Motagua fault system to the north, similar to geodetically-measured active deformation observed
35 east of the Guatemala City graben. Four new $^{40}\text{Ar}/^{39}\text{Ar}$ dates and correlation of tephra deposits
36 suggests that faulting was active during the Pliocene, but ceased eastward towards the Guatemala
37 City graben over time. From west to east, fault cessation occurred before the deposition of the
38 Los Chocoyos ash (84 ka) and E tephra (51 ka). Faulting just west of the Guatemala City graben
39 appears to be active, where a major fault cuts the most recent Amatitlan tephra. Based on this
40 data, we propose a time-progressive strain model for deformation related to North America-
41 Caribbean plate interactions, whereby distributed elongation of the westernmost Caribbean plate
42 occurred during the Pliocene but localized mostly within the Guatemala City graben and nearby
43 faults during the Quaternary. Our model supports that: 1) The Guatemala City graben is
44 effectively the western limit of the Caribbean plate; and 2) Western Guatemala, which used to be
45 the trailing edge of the Caribbean plate, has been transferred to the forearc region.

46

47

48

49

50 **1 Introduction**

51 One implication of the plate tectonics paradigm is the existence of triple junctions, where
52 the boundaries between three plates intersect (Morgan, 1968). McKenzie & Morgan (1969) first
53 proposed methods to determine whether the geometry of a triple junction will remain stable or
54 change over time based on the type and geometry of the intersecting plate boundaries (also see
55 York, 1973; Cronin, 1992). Their work has proved useful for understanding the kinematics and
56 geometric evolutions of most oceanic triple junctions, where the intersecting plate boundaries
57 and plate kinematics are both well defined. On the continents, where active deformation is often
58 distributed over wide areas, identifying triple junctions and how they evolve with time has
59 proved more challenging.

60 In Central America, studies have proposed the existence of a triple junction between the
61 North America, Caribbean, and Cocos plates, where the North America-Caribbean strike-slip
62 boundary terminates on land just east of the Middle America trench (Fig. 1; Pflafker, 1976;
63 Lyon-Caen et al., 2006; Alvarez-Gomez et al., 2008; Phipps Morgan et al., 2008; Authemayou et
64 al., 2011; Franco et al., 2012). Following the February 4, 1976 Motagua fault earthquake
65 ($M_w=7.5$), which killed or injured 2% of the population of Guatemala and left another 20% of the
66 population homeless, Plafker (1976) outlined several models for the plate boundary geometry
67 and associated deformation of this system. Some of these models are still debated, and they
68 address the broad continental deformation zone with left-lateral slip across the Polochic-Motagua
69 faults of Guatemala and distributed extension in southern Guatemala and western Honduras (Fig.
70 1; Muehlberger and Ritchie, 1975; Plafker, 1976; Burkart, 1978; 1983).

71 The introduction of geodesy as a means to define the regional crustal velocity field
72 enabled studies of the seismic cycles of the major active faults and the related regional

73 deformation. Lyon-Caen et al. (2006) focused on the seismically active Polochic-Motagua fault
74 zone (Fig. 1), which accommodates North America-Caribbean plate motion. The velocity field
75 strongly indicates that most or possibly all motion along the Polochic-Motagua fault zone is
76 transferred northward onto reverse faults and strike-slip faults in southern Mexico *and* southward
77 to north-striking grabens in western Honduras and southern Guatemala (Lyon-Caen et al. 2006).
78 Subsequent GPS measurements across the Salvadoran and Guatemalan volcanic arcs (Correa-
79 Mora et al., 2009; Alvarado et al., 2011; Franco et al., 2012) show that the Central America
80 forearc translates rapidly westward as a rigid or semi-rigid sliver (Fig. 1). Faults along the
81 volcanic arc accommodate this forearc motion and intersect the Polochic-Motagua fault zone to
82 the west, at a diffuse continental triple junction near the Mexico/Guatemala border. Recent work
83 by Ellis et al. (2018, 2019) increases the geodetic resolution of northern Central America,
84 including western Guatemala which previously had very few GPS sites. The available geodetic
85 measurements indicate that the Central America forearc west of the Guatemala City graben and
86 other areas of western Guatemala move nearly with the North America plate, with most
87 deformation focused farther to the east in central and eastern Guatemala and Honduras.

88 Based on geodetic and structural data, multiple models have been proposed for Central
89 American plate interactions (e.g., Plafker, 1976; Burkart and Self, 1985; Guzman-Speziale et al.,
90 1989; Gordon and Muehlberger, 1994; Lyon-Caen et al. 2006; Phipps-Morgan et al., 2008;
91 Authemayou et al., 2011; Franco et al., 2012; Andreani et al., 2016; Alvarez-Gomez et al., 2019).
92 The recent model from Authemayou et al. (2011) proposes a progressive development for
93 deformation in Guatemala in the form of the “zipper” model, whereby the Central America
94 forearc progressively fuses to the North America plate as the Caribbean plate and a triple
95 junction move eastward. Further data and modeling by Alvarez-Gomez et al. (2019) produced a

96 kinematic model that supports the zipper model with additional focus on the forearc sliver. They
97 propose that the forearc is pulled to the northwest by the North America plate, but is also pushed
98 at the other end by the collision of the Cocos Ridge in Costa Rica. Additionally, their model
99 indicates that the forearc sliver undergoes slight counterclockwise rotation at the northwestern
100 end to parallel North America velocity directions. Within this model, western Guatemala is the
101 next region to be affected by “zippering” of the forearc to North America. Western Guatemala,
102 however, is fairly inactive and it is unclear if it still belongs to the extending Caribbean plate.

103 In this contribution, we document the timing and deformation of fault systems in western
104 Guatemala, in an area west of the Guatemala City graben. Our estimates of timing of fault
105 activity are based on stratigraphic correlation and four new $^{40}\text{Ar}/^{39}\text{Ar}$ dates, with each one
106 constraining fault movement related to deformation between the Polochic-Motagua fault system
107 and the volcanic arc-forearc sliver. Structural observations from a new, well exposed outcrop
108 (Xenacoj) just west of the Guatemala City graben are used to understand deformation
109 immediately west of the Guatemala City graben. A new regional GPS velocity field derived from
110 1993-2017 data from Ellis et al. (2018, 2019) and updated with more recent data from campaign
111 sites in southern Guatemala and western El Salvador creates the framework for our interpretation
112 (Garnier et al., 2020 and Appendix A.1 in the supplemental material). Synthesizing this
113 information, we conclude that deformation in western Guatemala was more distributed in the
114 Pliocene, and is progressively becoming localized in the Guatemala City graben with diffuse
115 deformation in the surrounding area. These data suggest that Guatemala City graben best
116 approximates the present location of the triple junction, between the North America, Caribbean,
117 and forearc sliver plates. As a result, we propose a “localizing dashpot” model for deformation
118 associated with the North America-Caribbean plate interactions in Central America, in which

119 strain is progressively localized along the terminations of the Motagua and Jalpatagua faults, into
120 the Guatemala City graben region.

121

122 **2 The western Guatemala wedge**

123 Western Guatemala is in close proximity to the continental triple junction, but few
124 structural and geodetic data have been reported from this region, most likely due to safety
125 concerns and sparse, weathered outcrops. This observation is specifically true for an area that
126 we define as the “western Guatemala wedge” (red outline in Fig. 1), which is bounded to the
127 north by the Polochic-Motagua fault system, to the south by the volcanic arc, and to the east by
128 the Guatemala City graben.

129 Williams (1960) was first to geologically characterize western Guatemala and provides
130 broad lithology and structural descriptions for different regions within the western Guatemala
131 wedge. Later work focused on mapping and characterization of the Quaternary tephra
132 stratigraphy across Guatemala (Koch & McLean, 1975) and the volcanic arc and its related
133 deposits, with particular focus on the Atitlan caldera region (Clohan & Reynolds, 1977; Eggert &
134 Lea, 1978; Holekamp, Larson & Lundstrom, 1978; Hughes, 1978; Newhall, 1987; Rose et al.,
135 1979; 1987; 1999; Drexler et al., 1980). These studies mapped and defined the major Quaternary
136 tephras as they extend from the volcanic arc and into the western Guatemala wedge (Fig. 2).
137 These deposits include the Los Chocoyos ash (84 ka) from the Atitlan caldera, the most
138 prominent and wide-spread ashflow tephra across Guatemala and Central America that can
139 exceed 200 m in thickness in basins north of the Atitlan caldera. Neogene and older deposits are
140 only defined by broadly defined units near the volcanic arc (Fig. 2; Reynolds, 1977; 1980).

141 While structures were also mapped along the volcanic arc surrounding volcanic centers within
142 these studies, structural work has rarely extended into the wedge.

143

144 2.1 Geodesy

145 The framework for the present-day tectonics of our study area is defined by modeling of
146 a 200+ station GPS study in northern Central America and southern Mexico (Ellis et al., 2019)
147 and a recent update that assimilates new measurements from ~15 GPS sites in southern
148 Guatemala and western El Salvador (Garnier et al., 2020 and Appendix A.1 in the supplemental
149 material). Whereas some previous studies defined the western Guatemala wedge as part of the
150 Caribbean plate (Guzmán-Speziale et al., 1989; 2000, Lyon-Caen et al., 2006; Alvarez-Gomez et
151 al., 2008; Rodriguez et al. 2009; Authemayou et al., 2011; Franco et al, 2012), elastic block
152 modeling of the two new velocity fields indicates that the GPS sites in this wedge move with the
153 forearc sliver; these velocities are also similar to stations on the North America plate (Figs. 3A,
154 3B). Specifically, both regional block models indicate that sinistral slip rates across the
155 Polochic-Motagua fault system decrease from 11-13 mm yr⁻¹ just north and west of the
156 Guatemala City graben to 3 mm yr⁻¹ or less along the Motagua Fault directly west of the
157 Guatemala City Graben and the Polochic fault at the northern limit of the western Guatemala
158 wedge (Fig. 3A and Fig. 6B in Ellis et al. 2019). Both models also predict ~7-8 mm yr⁻¹ of
159 dextral slip along the Jalpatagua fault east and south of the Guatemala City graben, diminishing
160 to no detectable slip across faults in the volcanic arc immediately west of the Guatemala City
161 graben (Fig. 7B in Ellis et al. 2019 and Fig. 3B in Garnier et al., 2020). Both models thus
162 identify the Guatemala City graben as a critical, terminal structure within a broad extending
163 region east of the graben.

164 In accord with the above, GPS measurements at >40 sites within the wedge clearly reveal
165 14 ± 1 mm yr⁻¹ (95% uncertainty) of ~E-W elongation distributed unevenly across a 600-700-km-
166 wide zone in central and eastern Guatemala (Fig. 3B and Fig. 6B in Ellis et al. 2019). The more
167 recent Garnier et al. (2020) GPS velocity field (Fig. 3A; 3B), which is less noisy in our study
168 area than the earlier Ellis et al. velocity field, reveals two features of particular relevance to this
169 study. First, 10 ± 2 mm yr⁻¹ or 70% of the total elongation within the ~600-km-wide extending
170 wedge occurs across or within a few tens of km of the Guatemala City graben. Second, the E-W
171 elongation rate west of the Guatemala City graben slows dramatically (Fig. 3B), to only 2-3 mm
172 yr⁻¹ within 50 km west of the graben, where the Xenacoj outcrop referenced below is located,
173 and to no discernible deformation farther west. The GPS data thus suggest that the western
174 Guatemala wedge moves with the forearc sliver and North America plate to within the nearest 2-
175 3 mm/yr (Fig. 3A) and no longer deforms at distances greater than 40-50 km west of the
176 Guatemala City graben (Fig. 3B).

177 Based on the geodetic results described above, the Guatemala City graben closely
178 approximates the western limit of the Caribbean plate and is thus the best approximation of the
179 present triple junction between the North America, Forearc, and Caribbean (NAFCA) plates.
180 We suggest that the NAFCA terminology be adopted for this system as the forearc sliver is the
181 prominent third plate of the system, rather than the Cocos plate. The geodetic data conclusively
182 demonstrate that a North America-Caribbean-Cocos triple junction near or offshore from the
183 Guatemala/Mexico border does not exist (e.g., Ellis et al. 2019).

184

185 2.2. Observations of faulting in the western Guatemala wedge

186 Faulting is commonly observed within the western Guatemala wedge, even though the
187 recent GPS velocity field indicates that this region is generally not actively deforming. Due to
188 the highly vegetated environment of western Guatemala and sparse outcrops, our approach was
189 to characterize deformation in recently exposed road cuts (Fig. 4). We have concentrated our
190 efforts on four outcrops within the western Guatemala wedge. Three of the four outcrops are
191 capped with unfaulted units and consequently indicate that deformation is inactive or occurs at
192 very low strain rates at these sites. Additionally, these four outcrops form an east to west
193 transect and fall into different geomorphic regions of western Guatemala.

194 *Xenacoj, Location 1.* The Xenacoj outcrop occurs west of the Mixco fault, the western
195 fault of the Guatemala City graben, and south of the Motagua fault. Within this region, steep
196 valleys cut through thick volcanic deposits south of the Motagua fault (Fig. 4). In general, very
197 little work has been published for this area. Ritchie (1975) mapped the San Juan Sacatepéquez
198 quadrangle, which includes the Xenacoj outcrop, but only provided basic delineations of
199 Neogene and Quaternary formations. Mapping of Quaternary units suggest that these deposits
200 originated from the Amatitlan caldera to the southeast, as well as the widely distributed 84 ka
201 Los Chocoyos ash from the Atitlan caldera to the west (Koch and McLean, 1975; Rose et al.,
202 1979; 1987; 1999; Drexler et al., 1980; Wunderman & Rose, 1984; Fig. 2).

203 Construction of a new highway near Santo Domingo Xenacoj, ~10 km west of the Mixco
204 fault, exposed nearly 3 km of outcrop containing extensive faulting and numerous tephra and
205 reworked deposits (Location 1, *Xenacoj*; Figs. 2, 5A). One major fault, striking 124°, cuts nearly
206 40 m of outcrop and extends into the uppermost soil horizon. This major fault places a massive
207 biotite-rich crystal vitric tuff (footwall block; sample 17JF65S in Table 1) adjacent to a younger
208 series of faulted and unfaulted tephra, reworked sediments, and paleosols (hanging wall block).

209 The biotite-rich crystal vitric tuff is heavily fractured, altered, and contains large blocks of biotite
210 porphyry. Additionally, there is vertical variation in the igneous character of the deposit, more
211 lava like at the bottom and more pluton-like at the top, as well as less alteration at the bottom
212 than top. While none of the deposits can easily be linked to the known stratigraphy by
213 appearance, Williams (1960) and Ritchie (1975) briefly note a biotite-rich tuff that underlies
214 much of this area. Offset markers and fault drag indicate normal-sense, down to the SW,
215 movement of the main fault (Fig. 5A).

216 Faulting within the hanging wall was documented along two transects, which capture a
217 normal faulting event in the hanging wall that is capped by an erosional unconformity and a thick
218 sequence of unfaulted volcanic and reworked deposits ($n = 75$, average trend = 300° ; Fig. 5A).
219 The minor faults record tens of centimeters to meters of normal-sense offset. Slickenlines were
220 only observed along six fault planes in Transect A (11% of fault planes), with four slickenlines
221 with pitches ranging from $53\text{-}90^\circ$ and two slickenlines pitching less than 25° . To constrain fault
222 timing, three tephra deposits were sampled for $^{40}\text{Ar}/^{39}\text{Ar}$ dating and are described below (Table
223 1). Besides this outcrop, only sparse faulting was observed along other minor roadcuts or
224 quarries within this region.

225 *Tecpan.* The Chimaltenango basin extends between the Atitlan Caldera and the
226 Guatemala City graben, north of the volcanic arc (Fig. 4). The basin is characterized as a flat
227 plain with deep river valleys, often containing thick deposits of the Los Chocoyos tephra
228 overlain by post-Los Chocoyos sediments (Clohan & Reynolds, 1977). Other tephra deposits
229 from the Atitlan and Amatitlan calderas, as well as other smaller sources, also cover this area
230 (Fig. 2).

231 A large roadcut south of the city of Tecpan exposes normal faults in a section of red
232 volcanic sediments that are capped by thin and unfaulted, white tephra layers (Location 2
233 *Tecpan*, Fig. 2, 5B). An irregularly shaped intrusion is also exposed on the SE end of the
234 outcrop. Faults contain two orientations, a dominant orientation of $\sim 350^\circ$ and a secondary
235 orientation of 055° ($n = 14$, Fig. 5B). Faults record tens of centimeters to meters of normal
236 offset. No slickenlines were observed on fault planes. Mapping and descriptions by Clohan and
237 Reynolds (1977) identify the red sediments as reworked deposits of the Los Chocoyos tephra
238 (after 84 ka). The three white tephra layers that overlie faulted deposits were sampled for
239 geochemistry and unit correlation analysis (samples WH19S7, WH19S8, WH19S9; Table 1).

240 *Nahuala*. The area northwest of the Atitlan caldera contains volcanic lavas and
241 pyroclastic flows, tephra deposits, and structures related to the Atitlan caldera, as well as other
242 sources within the volcanic arc (Fig. 4). The exact stratigraphy is difficult to distinguish due to
243 numerous, small local Neogene and Quaternary volcanic deposits. However, the area
244 surrounding the Atitlan caldera is more thoroughly documented than any other area in western
245 Guatemala, with basic unit descriptions reported (Williams, 1960; Clohan & Reynolds, 1977;
246 Eggert & Lea, 1978; Holekamp, Larson & Lundstrom, 1978; Hughes, 1978; Newhall, 1987;
247 Rose et al., 1987).

248 Faults are observed in a roadcut approximately 14 km northwest of Lake Atitlan,
249 southwest of the city of Nahuala, in a highly indurated section of lahar flows and pebble/cobble
250 conglomerates capped by an unfaulted basalt/andesite flow (Location 3, *Nahuala*; Fig. 4; 5B).
251 Fault strikes vary between 300° and 355° and normal-sense fault offsets ranging from
252 centimeters to meters ($n = 14$). No slickenlines were observed on fault planes. A study by
253 Eggert & Lea (1978) map the faulted units as Neogene reworked deposits and describe a few

254 basalt flows in the area. An unfaulted, basalt/andesite flow caps the outcrop and the surrounding
255 area (sample 14GM14, Table 1). Further, unfaulted, thin white tephra deposits overlie the flow.

256 *Ilotenango*. The northwestern portion of the western Guatemala wedge is marked by
257 linear, deep-cut river valleys that extend southeastward from the mountains just south of the
258 Polochic fault (near Huehuetenango), to the tip of the Motagua fault, and southward to ~30 km
259 behind the volcanic arc (Figs. 1, 4). River valley orientations change slightly across the area
260 from ~045°-trending near Huehuetenango to ~032°-trending north of Lake Atitlan. The physical
261 and geomorphic map of Guatemala (Alvarado Cabrera & Herrer Ibáñez, 2001) describes the
262 river valleys as being fault-controlled related to movement on the Motagua fault. No other study
263 analyzes the parallel river valleys of the region.

264 Williams (1960) describes that much of the river valley region is blanketed by a pink-
265 topped tephra, which matches descriptions and mapping of the Los Chocoyos tephra by Rose et
266 al. (1979; 1987; 1999) and Wunderman and Rose (1984). The Los Chocoyos tephra is underlain
267 by Neogene tuffaceous sediments and conglomerates with dips as great as 30°. The Los
268 Chocoyos ash is thickest in this region and can reach up to 100's meters in thickness in the deep
269 valleys (Rose et al., 1979; 1987; 1999; Drexler et al., 1980; Wunderman & Rose, 1984). Other
270 tephra from the Atitlan caldera also extend throughout the area (Fig. 2).

271 Minor normal faulting is exposed on the eastern side of this region, in a small roadcut
272 south of the town of San Antonio Ilotenango (Location 4, *Ilotenango*; Fig. 4; 5B). Normal faults
273 were recorded in a series of tan, fine-grained, indurated, reworked volcanic sediments, that are
274 overlain by a thick, unfaulted white tephra (Fig. 5B). Fault orientations are nearly parallel river
275 valley orientations with strikes ranging from 020° to 030°, with tens of centimeters to meters of
276 normal offset (n = 25). One slickenline was observed at this outcrop, with a pitch of 77°. The

277 overlying white tephra contains large white pumice blocks and charcoal logs and reaches a
278 thickness of at least 100 m in nearby exposed quarries and valleys. These observation match
279 descriptions and mapping of the Los Chocoyos tephra and a sample was collected for
280 geochemical analysis (sample 14GM7, Table 1).

281

282 **3 Methods**

283 3.1. Minor Fault Analysis

284 At each outcrop, faults (orientations, visible slickenlines, and fault separations on the
285 outcrop face) were recorded along a transect of measured length, along with nearby bedding
286 orientations. We observed very few slickenlines along fault surfaces at our outcrops: six
287 slickenline measurements along Transect A at Xenacoj and no slickenlines observed along
288 Transect B; no slickenlines were observed at Tecpan and Nahuala; and one slickenline
289 measurement at Ilotenango. Marker beds indicate a normal sense of motion across nearly all
290 fault planes and the majority of sparse slickenline data indicates down-dip movement.
291 Therefore, we assume normal, down-dip movement for our collected fault data and this
292 assumption was applied to the methods that follow. Samples were also taken for unit correlation
293 purposes (e.g., the highest faulted unit and the lowest unfaulted unit, so fault timing could be
294 constructed). Samples were not gathered from reworked deposits, which limits determining fault
295 timing constraints at some outcrops. All gathered samples, fault data, and outcrops are briefly
296 described in Table 1 and Figures 5A and 5B.

297

298 3.2. Means and statistical tests

299 All collected normal fault data (poles to the plane) are displayed in Figure 6A to visualize
300 the variation of fault orientations from the four outcrops. To explore the data sets with statistical
301 methods, we applied methods explained in Davis and Titus (2017). Specifically, we determined
302 a mean and 95% confidence ellipse of the bootstrapped means for each data set, using their code
303 package for R. For each location, the fault mean was calculated by computing the eigenvector
304 with the greatest eigenvalue from a scatter matrix of the pole data (*lineProjectedmean*). The
305 secondary fault set for Tecpan (open circles in Figure 6A) was not included for the Tecpan mean
306 calculation, or the following bootstrap application. The statistical method of bootstrapping was
307 applied to each data set to compute 10,000 means from 10,000 synthetic data sets that were
308 created by sampling with replacement (*lineBootstrapInference*). The synthetic data sets will
309 have duplicates and omissions of the original data set and will generate slightly different means.
310 This approach aims to simulate the variation of means from the larger fault population (all faults
311 in the field). An elliptical confidence region was generated for each location that encompasses
312 95% of the bootstrapped means and serves as a method to compare the individual data sets. We
313 observe that no ellipses overlap among the four data sets (right stereonet, Fig. 6), indicating that
314 the means are statistically different for each area and fault populations are different.

315

316 3.3. Strain

317 One-dimensional strain, elongation, was calculated for each of the four outcrops
318 containing normal faults observed in western Guatemala. The applied method focuses on
319 calculating true displacement across faults, regardless of transect orientation (following methods
320 outlined by Titus et al., 2007; Xu et al., 2007; Xu et al., 2009). The same approach was applied
321 by Garibaldi et al. (2016) in the Salvadoran volcanic arc. A more thorough explanation can be

322 found in Garnier et al. (2020) as applied to faulting in eastern Guatemala. In general, the
323 direction of maximum elongation is determined by finding the orientation that maximizes the
324 combined apparent heave of all faults along a transect, using the ratio between apparent heave
325 and total heave (h_{app}/h_{total}). A graphical representation of this relationship for all outcrops is
326 shown in Figure 7A.

327 For each transect, we calculated elongation based on measured faults (termed
328 “elongation”), and then revised the calculation to include the collective offset of small,
329 unobservable faults (termed “revised elongation”) (Marrett et al., 1991; 1992; Walsh et al., 1991;
330 Gross and Engelder, 1995). Faults with orientations within 50° of the maximum elongation were
331 used for each estimation. Bounding faults were excluded from the estimation to maintain an
332 unbiased calculation. To calculate elongation from observable faults, the true horizontal heave
333 was calculated for each fault and projected onto the maximum elongation direction. All
334 horizontal heaves were combined to determine the collective heave in the direction of maximum
335 elongation and the percentage of elongation (Table 2).

336 To include the effect of small faults, frequency-displacement plots (log of cumulative
337 frequency versus log of fault displacement, with 1 being the largest fault to n being the smallest
338 fault) were generated to show the fractal quality of fault populations (Fig. 7). A slope was fitted
339 to the linear portion of the frequency-displacement plot, representing intermediate faults that are
340 often observed at outcrop level. The slope value (C) was used to compute the horizontal
341 displacement due to small, unobservable faults (e.g., Gross and Engelder, 1995). The heave
342 from small faults was added to the originally calculated heave and used to determine a revised
343 percent elongation (Table 2, Fig. 8).

344 Schematic diagrams of the original and resultant maximum elongation transects are
345 shown in Figure 8, while Figure 10 shows the maximum elongation direction (white arrows) in
346 map view for each location. In general, there is a range of maximum elongation directions,
347 varying from E-W to NNE-SSW, and elongation amounts, varying from 0.64% - 15.8%,
348 determined from these minor fault arrays.

349

350 3.4. Unit correlation

351 With elongation directions and amounts estimated from fault data, identifying faulted and
352 unfaulted lithologies is needed to develop the deformational history of western Guatemala. Field
353 evidence (unit appearance, thickness, location, and stratigraphic relationships to marker units)
354 and pumice mineralogy (particularly the presence and amount of mafic phenocrysts) are the two
355 best criteria for identifying and correlating units to published descriptions, tephra isopach maps,
356 and geologic maps (Koch, 1970; McLean, 1970; Koch & McLean, 1975; Rose et al., 1981). For
357 the Quaternary deposits, field evidence was used in combination with XRF data and pumice
358 mineralogy from cleaned pumice fragments to link deposits to major Quaternary tephras. For
359 Neogene deposits, field evidence was the main method of unit correlation due to the lack of
360 detailed data and analyses in the literature (Reynolds, 1977; 1980). Additionally, four samples
361 were used for $^{40}\text{Ar}/^{39}\text{Ar}$ age analysis, to further correlate to the known stratigraphy and/or to
362 determine the age of a previously undated unit. Data from these analyses are presented in Tables
363 1 and 3.

364

365 3.4.1. Pumice Geochemistry and Mineralogy

366 Major and trace element geochemistry of eight tephra samples was obtained by XRF
367 analysis on washed pumice fragments (conducted by the Geoanalytical lab at Washington State
368 University; Table 3A). While most researchers conducting tephra correlation studies analyze
369 glass geochemistry by ICP-MS, the biggest drawback to this technique is low discrimination
370 between tephtras of the same or related sources, which is the situation in Guatemala with the two
371 nearby rhyolitic sources of Atitlan and Amatitlan (Fig. 2; Sarna-Wojcicki, 2000). Therefore,
372 bulk pumice fragment geochemistry was used to compare XRF data to those in the literature.
373 Similarity coefficients were calculated between the eight tephra samples and ten Quaternary
374 tephtras that have documented geochemistry in the literature (Table 3B; Similarity coefficient
375 equation: Borchardt & Harward, 1971; Sarna-Wojcicki et al., 1984; Sarna-Wojcicki, 2000;
376 Published XRF data: Wunderman & Rose, 1984; Rose et al., 1987). Similarity coefficients were
377 calculated using the normalized weight percent of the following major elements: SiO₂, FeO,
378 TiO₂, Al₂O₃, MgO, CaO, Na₂O, K₂O, and P₂O₅; and ppm of following trace elements: Sc, Ba,
379 Rb, Sr, Zr, and La (Table 3B). Tephra pairs with the highest similarity coefficients were
380 considered as potential correlations and compared to the field and dating evidence (Table 1).

381 In addition to XRF analysis, pumice mineralogy was determined for five tephra samples.
382 A mineral count analysis was conducted on crushed, clean pumice fragments, and results
383 compared to previous work by Koch (1970), McLean (1970), and Koch & McLean (1975).
384 Weight percentages of glass, felsic minerals, and mafic minerals, as well as mineral counts of the
385 mafic phenocrysts, are included in Table 1 under Mineralogy.

386

387 3.4.2. ⁴⁰Ar/³⁹Ar dating

388 $^{40}\text{Ar}/^{39}\text{Ar}$ dating was conducted on one tephra (pumice fragments from 17JF56R), one
389 crystal-rich tuff (17JF56A), one andesite porphyry (17JF56S), and one basalt flow (14GM14M),
390 all collected at faulted outcrops (Table 1). Plagioclase (250-500 μm) was isolated from the
391 tephra, tuff, and porphyry samples. Groundmass (180-250 μm) was isolated from the basalt
392 flow. The groundmass was treated with 1.2M HCl in an ultrasonic bath for 10 minutes, and then
393 rinsed thoroughly with deionized water. Because some of the groundmass still showed evidence
394 of alteration, additional ultrasonic leaching was done in a 3M HCl solution for 15 minutes
395 followed by ultrasonic rinsing in deionized water and hand picking under a binocular
396 microscope. The plagioclase was treated with 10% HF in an ultrasonic bath for 5 minutes, and
397 then rinsed thoroughly with deionized water. The purified groundmass and plagioclase separates
398 were wrapped in an aluminum foil packet and irradiated with 1.1864 Ma Alder Creek sanidine
399 (ACs). At the University of Wisconsin-Madison WiscAr Laboratory, ~15 mg of groundmass
400 was incrementally heated using a 50W CO₂ laser and single crystal total fusion experiments were
401 performed on the plagioclase from the other three samples. All analyses were done using a
402 Noblesse 5-collector mass spectrometer following the procedures in Jicha et al. (2016). Results
403 are summarized in Table 4 (complete data is available in Appendix A.2 in the supplemental
404 material).

405

406 3.5. Elongation Rate

407 We calculated elongation rates for each of the four outcrops using: 1) the estimated
408 elongation; and 2) ages of faulted and unfaulted deposits which delimit the timing of
409 deformation. To determine elongation rate, the amount of added length for each outcrop (dFr in
410 millimeters, Table 2; 4) was divided by the estimated time span of active faulting (age of

411 youngest faulted unit minus overlying, unfaulted deposit, in years; Table 5). Elongation rates
412 were similarly calculated in the El Salvador fault zone by Garibaldi et al. (2016). Since we can
413 only determine the end points of the period of active faulting, all elongation rates are minimums
414 (all data displayed in Table 5).

415

416 **4 Results**

417 4.1. Xenacoj outcrop

418 Results from the minor fault analysis and $^{40}\text{Ar}/^{39}\text{Ar}$ dating of three samples from the
419 Xenacoj outcrop, west of the Guatemala City graben, indicate that large volcanic and faulting
420 events occurred in this area during the Neogene and Quaternary. The height of the faulted
421 outcrop indicates that the main fault (striking 124°) accommodated at least 40 m of normal
422 movement to the southwest. Folding of the hanging wall deposits also suggests that the main
423 fault may have a listric shape in the subsurface, while thickening of individual layers towards the
424 main fault suggests periods of syndepositional faulting.

425 Minor faults measured along two transects estimate that 2.1% and 11.5% of $033^\circ/034^\circ$ -
426 directed elongation occurred within the hanging wall block (Fig. 8). The difference in estimated
427 elongations is most likely attributed to one large area of distributed strain in Transect A, where it
428 was difficult to determine precise fault planes and offsets. Transect B only contained clear fault
429 planes and offsets. Therefore, we suggest that the estimated 11.5% elongation from transect B,
430 although in younger sediments, is more representative of the elongation that occurred prior to the
431 overlying unconformity. Additionally, faulting from both transects appear to represent the same
432 deformational event (Fig. 4A).

433 Observed deposits do not correlate to any of the known tephtras in the literature, yet
434 suggest that large eruptive events have occurred from unknown, nearby source(s). $^{40}\text{Ar}/^{39}\text{Ar}$
435 dating of the three samples gave weighted mean ages of 9.115 ± 0.008 Ma (Late Miocene) for
436 the massive biotite-rich crystal vitric tuff in the footwall (17JF56S), 1.495 ± 0.057 Ma
437 (Quaternary) for the lowest, faulted tan vitric tuff in the hanging wall (17JF56A, Unit 1), and
438 1.145 ± 0.061 Ma (Quaternary) for the highest, faulted grey pumice lapilli tuff in the hanging
439 wall (17JF56MR, Unit 4) (Fig. 9A; Table 4). Additionally, plagioclase from one tephtra
440 (17JF56J) sampled near the surface (Unit 4) lacked radiogenic Ar. However, this sample appears
441 geochemically similar to the E tephtra from the Amatitlan caldera. The age of the E tephtra from
442 Amatitlan is estimated at 51 ka, based on sedimentation rates in ocean cores (Schindlbeck et al.,
443 2018).

444 By combining the structural and stratigraphic data, faulting in Transects A and B
445 occurred in the Quaternary, after deposition of 1.145 ± 0.061 Ma grey tuff and before deposition
446 of the thick unfaulted sequence of tephtras and sediments. Since we are unable to date the
447 stratigraphically lowest members of the unfaulted sequence, fault timing cannot be constrained
448 beyond using the youngest unfaulted 51 ka white tephtra deposited near the surface, which would
449 provide a window of ~ 1.1 Ma for the Transect B recording 11.5% elongation, which indicates a
450 minimum strain rate of <0.01 mm yr⁻¹ for the outcrop (Table 5). A more detailed deformational
451 and stratigraphic history of this outcrop is outline in Appendix A.3 of the supplemental material.

452

453 4.2. Tecpan outcrop

454 Minor faulting at the Tecpan outcrop suggests 0.64% of elongation occurred at a
455 direction of 083° , based on the dominant \sim N-NNW normal fault set (Fig. 8). A primary N-NNW

456 fault set and secondary NE-striking faults parallel other lineaments identified by Clohan &
457 Reynolds (1977) within this area. As previously stated, faulting occurred in post-Los Chocoyos
458 reworked deposits (after 84 ka). Similarity coefficients suggest that the overlying, unfaulted
459 tephras are geochemically similar to multiple Quaternary tephras. However, by eliminating
460 tephras older than the Los Chocoyos, we suggest that the lower two tephras best represent the C
461 and E tephras from the Amatitlan caldera (ages of 54 ka and 51 ka, respectively; Schindlbeck et
462 al., 2018, see Figure 3). The uppermost tephra could not be correlated to a post-Los Chocoyos
463 tephra based on the available data. Therefore, faulting in this area most likely occurred in a short
464 period during the Quaternary, between deposition of the Los Chocoyos and C tephras (84 ka and
465 54 ka, a 30 ka span; Fig. 10). If the timing estimate is correct, it indicates a very low strain rate
466 of 0.045mm yr^{-1} of 083-elongation at the faulted outcrop (Table 5).

467

468 4.3. Nahuala outcrop

469 From minor faulting within the Nahuala outcrop, we estimate 4.2-4.7% elongation
470 occurred in a maximum elongation direction of 056° (Fig. 8). The dominant presence of
471 andesitic material in the faulted, reworked lahar and conglomerate deposits suggest that they
472 belong to the Balsamo formation, extending from Late Miocene through the Pliocene. This
473 interpretation agrees with mapped Neogene lahar deposits by Eggert (1978). The overlying
474 basalt flow did not yield a plateau, but most of the heating steps give ages between 3.3 and 3.2
475 Ma (Fig. 9B; Table 4), which we use as an approximation for its age. This sample closely
476 matches descriptions of the Tertiary Cerro Jox Andesite flow of Eggert (1978). Thin white,
477 unfaulted tephras overlie the flow and are most similar geochemically to the I falls (>40 ka) from
478 Atitlan (Rose et al., 1999) and fall within the mapped depositional area of this tephra. Therefore,

479 NE-elongation at the Nahuala outcrop likely took place in the Miocene, after the Middle
480 Miocene reworked deposits, and ceased before deposition of the ~3.2 Ma flow, with no obvious
481 faulting of Quaternary deposits in the area (Fig. 10). If we use the Late Miocene boundary for
482 the Balsamo formation (11.14 Ma) and the range of elongation amounts, it indicates an
483 elongation rate of $<0.001 \text{ mm yr}^{-1}$ (Table 5). This estimate is very conservative without a more
484 precise age for the faulted deposits.

485

486 4.4. Ilotenango outcrop

487 Results from the minor fault analysis at the Ilotenango outcrop indicate that 15.8%
488 elongation has occurred in a maximum elongation direction of 112° , which is roughly
489 perpendicular to the orientation of nearby river valleys (Fig. 8). Field evidence, geochemistry,
490 and pumice mineralogy indicate that the overlying, unfaulted white tephra correlates to the Los
491 Chocoyos ash, which has an assigned age of $84 \pm 5 \text{ ka}$ based on oxygen-isotope stratigraphy in
492 ocean cores in which it is found (Drexler et al., 1980). Faulted deposits are most likely Neogene
493 in age, based on descriptions by Williams (1960), but a more precise age could not be
494 determined due the reworked nature of the deposits and the lack of individually defined Neogene
495 deposits in the literature. If the Neogene deposits are assigned to the Balsamo formation (Upper
496 Miocene to Pliocene) or the Chalatenango formation (Middle/Upper Miocene), faulting would
497 have occurred after 2.58 Ma or 5.33 Ma, respectively, and ceased by 84 ka (Fig. 10). A time
498 span of 1.74 – 5.2 Ma would indicate a slow elongation rate of $<0.001 \text{ mm yr}^{-1}$ for the transect.
499 If the elongation results from Ilotenango are applied to the entire region of linear river valleys
500 (15.8% elongation over ~40 km at an orientation of 112°), 6.32 km of added length would
501 indicate a minimum extension rate of 1.2-3.6 mm yr^{-1} for the region (Table 5).

502

503 **5 Discussion**

504 5.1. Timing of fault cessation

505 Combining the deformational histories of all four outcrops, faulting is oldest in the west
506 and youngest in the east across the western Guatemala wedge (Fig. 10). Faulting at Nahuala near
507 the volcanic arc suggests that the western Guatemala wedge was actively deforming in the
508 Pliocene, with fault cessation by ~3.2 Ma. The faulting at the Xenacoj outcrop also suggests
509 active deformation in the wedge during the early Quaternary, with movement of the main fault
510 during deposition of the 1.495 Ma and the 1.145 Ma tephra. After these faulting events, we
511 observe an eastward trend to fault cessations. Faulting ceased by 84 ka (Los Chocoyos ash) at
512 Ilotenango, our western most outcrop, by 54 ka (C tephra) at the central Tecpan outcrop, and
513 faulting may still be active at the eastern most Xenacoj outcrop, as the main fault offsets the 51
514 ka E tephra and the youngest observed tephra (Fig. 10). The record of fault cessations progresses
515 eastward, towards the Guatemala City graben.

516

517 5.2. Elongation directions determined by fault arrays

518 From east to west, the minor fault analysis estimated NE-directed elongation (033°) at
519 Xenacoj, nearly E-W elongation (083°) at Tecpan, NE elongation (056°) at Nahuala, and ESE
520 elongation (112°) at Ilotenango (Fig. 10). The maximum elongation directions are variable, but
521 can be separated into roughly E-W (Tecpan and Ilotenango) and NE-SW (Nahuala and Xenacoj)
522 elongation directions.

523 While fault data from Tecpan and Ilotenango come from statistically different fault
524 populations (Fig. 6), we suggest that they both result from internal E-W elongation of the

525 western Guatemala wedge. E-W elongation at Tecpan is most similar to active E-W elongation
526 directions recorded in secondary faulting along the Jalpatagua fault to the east (Garnier et al.,
527 2020), as well as E-W extension observed in the GPS data across central and eastern Guatemala,
528 with a majority of the extension concentrated on the Guatemala City graben (Ellis et al., 2019;
529 Garnier et al., 2020).

530 The similar elongation directions could suggest that the western limit of the Caribbean
531 plate, the limit of active E-W elongation, extended into western Guatemala in the past. If so,
532 elongation was active on both sides of the Guatemala City graben, whereas now it is focused
533 primarily in the graben, as well as immediately to its west and the region to its east. While the
534 maximum elongation direction at Ilotenango is more inclined to the ESE, the deformation can
535 still be linked to internal E-W elongation of the Caribbean plate if we look at the curvature of the
536 Motagua- Polochic fault system. While the Motagua and Polochic faults are individually
537 oriented E-W across central and western Guatemala, the fault system is curved in map view.
538 That is, the faults collectively create a WNW-ESE-oriented end of the curve in western
539 Guatemala and an ENE-WSW-oriented end in eastern Guatemala/western Honduras. Work by
540 Burkart and Self (1985) and modeling by Rodriguez et al. (2009) suggest that elongation
541 directions within the Caribbean plate south of the fault system will parallel and rotate around this
542 curvature as the Caribbean plate moves eastward. This idea is supported by N-S grabens in
543 central Guatemala and NW-trending grabens and faults in western Honduras (Rogers et al.,
544 2002), and would explain the NE-trending river valleys and faults and the related ESE elongation
545 estimated at Ilotenango within the western Guatemala wedge.

546 NE-elongations at the Nahuala and Xenacoj outcrops are interpreted differently. NE-
547 oriented elongation (056) observed at Nahuala is similar to NE-elongations (ranging from 033 to

548 073) observed near the eastern termination of the Jalpatagua fault and within the El Salvador
549 fault zone. In both cases, the NE-oriented elongations result from distributed deformation
550 associated with dextral, obliquely divergence forearc movement (Garibaldi et al., 2016; Garnier
551 et al., 2020). Since the Nahuala outcrop is near the forearc boundary, a similar area of oblique
552 divergence could have occurred in the past along the volcanic arc west of the Guatemala City
553 graben. The distributed zones of deformation in El Salvador occur between adjacent strike-slip
554 faults. Since the distributed deformation of this area is similar to the El Salvador fault zone, it
555 suggests that a dextral fault – an extension of the active Jalpatagua fault – once continued along
556 the south side of the western Guatemala wedge within the active volcanic arc.

557 The NE-directed maximum elongation orientation (033) at the Xenacoj outcrop is slightly
558 different from Nahuala, but suggests elongation of the backarc towards the trench, perpendicular
559 to the Motagua- Polochic fault system and volcanic arc. Ritchie (1975) mapped other large
560 faults of this orientation in the area, indicating that the Xenacoj outcrop represents a regional
561 deformation pattern. With the western termination of the Motagua fault nearby, it is also
562 possible that faulting is related to the termination of this structure.

563 Overall, the elongation directions at Tecpan, Ilotenango, and Nahuala in the western
564 Guatemala wedge parallel active elongations directions estimated in central and eastern
565 Guatemala. With this evidence, we suggest that the internally deforming, trailing edge of the
566 Caribbean plate extended into western Guatemala when the extensional faulting took place.

567

568 5.3. Comparison of structural and geodetic strain rates

569 While many assumptions were made to estimate elongation and elongation rates at all
570 four outcrops (e.g., down-dip movement on faults; period of active faulting), we can still

571 compare the elongation rates to the current GPS study to infer about the past state of
572 deformation. The GPS data indicate that the trailing wedge of the Caribbean plate is internally
573 deforming at E-W elongation rates of 10 mm yr^{-1} across the Guatemala City graben and a slower,
574 constant rate surrounding the graben and into eastern Guatemala (Ellis et al., 2019; Garnier et al.,
575 2020). The estimated, ESE-directed elongation rate for Ilotenango/linear river valley region
576 ($1.2\text{-}3.6 \text{ mm yr}^{-1}$) from the Neogene to 84 ka is close to the distributed rate measured at locations
577 in eastern Guatemala, such as across the Ipala graben and the general diffuse deformation in
578 eastern Guatemala (Fig. 5B). It is important to emphasize that our lack of more precise fault
579 timing means that all elongation rates are minimums and true elongation rates could have been
580 higher. The Ilotenango elongation rate is estimated for a large region of distributed deformation,
581 similar to the current situation in eastern Guatemala. A higher overall distributed strain rate in
582 the past could indicate a slower rate across the Guatemala City graben and an overall more
583 distributed state of deformation across the western Caribbean plate. While deposition ages are
584 better constrained at Tecpan, the E-W extension strain rate of 0.045 mm yr^{-1} is much smaller than
585 the current elongation rates across the large grabens. However, Tecpan could indicate the lower
586 end of E-W strain rates across minor structures or small areas.

587 The slow elongation rates estimated from Xenacoj ($<0.01 \text{ mm yr}^{-1}$) and Nahuala (<0.001
588 mm yr^{-1}) likely underestimate the strain rate needed to create the observed deformations,
589 particularly the extensive faulting at Xenacoj. The lack of precise ages for reworked deposits
590 that would more accurately constrain rate estimates make it difficult to compare to the GPS data.
591 However, the current GPS data observes $2\text{-}3 \text{ mm yr}^{-1}$ of E-W extension within 50 km west of the
592 Guatemala City graben, which includes the Xenacoj outcrop. This observation supports our

593 observation that the main fault cuts all deposits, including the most recent Amatitlan tephtras, and
594 faulting is still active in this area.

595 Estimated elongation and elongation rates in western Guatemala suggest that the Polochic
596 fault and the volcanic arc were active structures during the period of active faulting. Currently,
597 there is 2-4 mm yr⁻¹ of sinistral movement estimated for the Polochic fault to the north (e.g., Ellis
598 et al., 2019), but it is unclear if a higher rate could have been present, or required, during the past
599 deformation. To the south, there is no measurable dextral strain across the volcanic arc west of
600 the Guatemala City graben (Ellis et al., 2019). Previous authors have mapped fragmented
601 lineaments parallel to the forearc boundary across the volcanic arc, but most are buried by the
602 nearby volcanic centers and their deposits (Newhall, 1987). Additionally, minor fault
603 orientations recorded within the Atitlan caldera are similar to minor fault sets measured along the
604 active forearc boundary in eastern Guatemala, the Jalpatagua fault (i.e., N-striking normal faults
605 and strike-slip fault sets following the Riedel shear model for dextral shear; Newhall, 1987;
606 Garnier et al., 2020). Minor faulting indicative of major dextral movement and the presence of
607 the Atitlan caldera (known to have three large caldera-forming events) along the now stable
608 volcanic arc may support past motion along this boundary, as calderas could have been
609 connected to movement on large strike-slip faults.

610

611 5.4. Geologic evidence for the NAFCA triple junction

612 The Guatemala City graben region is the current plate juncture between the North
613 America, forearc, and Caribbean plates (e.g., Ellis et al., 2019). The sinistral Motagua-Polochic
614 fault system forms the main boundary between the North America and Caribbean plates. Within
615 this system, two-thirds or more of the slip occurs on the Motagua fault, which ends ~25 km west

616 of the Guatemala City graben. There is abundant evidence of normal faulting south of the
617 Motagua fault in the western Caribbean wedge (Langer and Bollinger, 1979), including at the
618 Xenocoj outcrop.

619 Another way of evaluating the movement of the western Guatemala wedge is to
620 investigate its relation to the forearc. The dextral Jalpatagua fault in southeastern Guatemala is
621 the main boundary between the Caribbean plate and the forearc sliver. The western termination
622 of the Jalpatagua fault occurs at or near the Amatitlan caldera, at the southern end of the
623 Guatemala City graben (Garnier et al., 2020). There is no structure or geomorphic evidence for
624 an active fault that could be the continuation of the Jalpatagua fault west of the Amatitlan
625 caldera/Guatemala City graben. Therefore, both of the major Caribbean plate boundaries in
626 Guatemala - the Motagua and Jalpatagua faults - have geologic evidence of terminations near the
627 Guatemala City graben. Hence, the geologic and geodetic data indicate that the Guatemala City
628 graben and faulting immediately west of the graben are the current western limit of the
629 Caribbean plate. The Motagua and Jalpatagua faults, with opposing shear senses, act as the
630 margins of a “dashpot” that allows the Caribbean plate to move eastward. A dashpot is a
631 mechanical device that dampens or resists motion, consisting of a cylinder and moving piston
632 (schematic in Figure 11). In this analogy, deformation at the western end of the Caribbean plate
633 accommodates the gap that is created as the Caribbean plate “piston” moves outward (eastward)
634 constrained by the North America and forearc plate boundaries. Since a majority of the eastward
635 movement is accommodated across the Guatemala City graben, with distributed extension
636 surrounding the graben from just to its west to eastern Guatemala, the evidence supports that the
637 Guatemala City graben region currently acts as the NAFCA triple junction.

638 Although the sinistral Motagua and Polochic faults jointly accommodate North America-
639 Caribbean plate relative motion (Fig. 2), the former ends in an extensional zone to the south and
640 the latter in a contractional zone to the north. From a North American perspective, the Motagua
641 fault allows eastward movement of the westernmost Caribbean plate (Fig. 3B, Lyon-Caen et al.
642 2006; Ellis et al., 2019). Near Guatemala City, slip along the Motagua fault decreases rapidly as
643 the fault slip is transferred southward onto extensional faults in the westernmost part of the
644 Caribbean plate. In contrast, slip on the Polochic fault diminishes more gradually westward
645 (Ellis et al., 2019), and the fault motion is partitioned northward onto thrust and strike-slip faults
646 in the diffuse shortening zone of southern Mexico and northern Guatemala (e.g., Guzman-
647 Speziale, 2001; 2010).

648

649 5.5. Progressive localization and trailing edge “capture”

650 With the current western limit of the Caribbean plate occurring near the Guatemala City
651 graben, the evidence discussed above supports that the western limit of the Caribbean plate
652 extended into western Guatemala in the past (Fig. 11). Strain distributed across small structures
653 ceased towards the Guatemala City graben over 100 ka or more, which differs from the predicted
654 western Guatemala deformation from previous triple junction models. We propose an updated
655 model for plate interactions where distributed strain is localized over time towards the
656 Guatemala City graben and eastward movement of the trailing edge of the Caribbean plate
657 sutures western Guatemala to the forearc sliver.

658 During the Pliocene and part of the Quaternary, the trailing wedge of the Caribbean plate
659 extended from western Guatemala to western Honduras and underwent east-west elongation,
660 between the volcanic arc-forearc sliver and the Polochic-Motagua fault system (Fig. 11, upper

661 panel). The inference of a more spatially extensive wedge of distributed deformation is
662 supported by inactive faults in the western Guatemala wedge. For internal deformation to occur
663 in western Guatemala, the dextral forearc boundary had to extend into western Guatemala, with
664 movement along the now stable volcanic arc. It is unclear where to place the western limit of
665 distributed deformation during this spatially extensive deformation.

666 The same inference can be made for faulting in Honduras: Faults and grabens mapped in
667 western Honduras have become inactive (Rogers et al., 2002) with distributed elongation active
668 to its west in eastern Guatemala. Faults in western Honduras initiated around 10 Ma and were
669 active after 3.5 Ma (Rogers et al., 2002). These faults, however, are currently inactive as
670 constrained by the geodetic data of Ellis et al. (2019). This timing – active at 3.5 Ma but
671 currently inactive - coincides with our constraints for timing of western Guatemalan faults.
672 Faulting from western Guatemala to western Honduras accommodated overall E-W elongation
673 with smaller structures striking perpendicular to the curve of the Polochic-Motagua fault system.

674 With evidence of deformation ceasing in an eastward trend in the western Guatemala
675 wedge, we suggest that widespread, distributed strain of the Caribbean wedge progressively
676 localized towards the Guatemala City graben area and eastern Guatemala during the Quaternary
677 (Guatemala City and Ipala graben; Fig. 11, middle panel). Eastward cessation of faulting within
678 the wedge would also track an eastward stabilization of the volcanic arc as dextral motion
679 stopped. As deformation within the wedge and along the volcanic arc ceases in an eastward
680 fashion, inactive material of western Guatemala becomes essentially sutured to the forearc sliver.

681 This process of suturing is similar to the Authemayou et al. (2011) zipper model,
682 although different in detail. The Authemayou et al. (2011) zipper model predicts that the
683 Caribbean plate escapes between the North America plate and the forearc sliver as they suture

684 together. Our data in western Guatemala does not support this model, as the western Guatemala
685 wedge just ceases deforming. Rather, the western trailing edge of the Caribbean plate is
686 transferred, or captured, to the North America plate and/or forearc sliver as motion along the
687 volcanic arc and Polochic fault are significantly reduced (Fig. 7). A similar prediction of
688 material transfer of western Guatemala was made from the recent modeling study from Alvarez-
689 Gomez et al. (2019).

690 The new geodetic results demonstrate that strain localization and capture of western
691 Guatemala continued to the Guatemala City graben and area immediately west, the current
692 western plate boundary between North America, forearc, and Caribbean (NAFCA) plate
693 movements (Fig. 11, lower panel). However, minor distributed deformation is still observed in
694 structural and GPS data just west of the Guatemala City graben, as well as minor extension
695 across eastern Guatemala. Figure 11 portrays our strain localization model for NAFCA plate
696 interactions from ~4 Ma to present, incorporates many minor structures within the larger wedge,
697 and shows the current plate boundaries and new prominence of the Guatemala City graben.

698 Figure 11 forms the basis for the “localizing dashpot” model. In the past, when the
699 extensional deformation was more distributed from western Guatemala to western Honduras, the
700 kinematics require: 1) The presence of a right-lateral slip – on an arc-parallel fault – that
701 extended further west than the current Jalpatagua fault; and 2) More left-lateral slip on the
702 western end of the Motagua-Polochic system, presumably on the Polochic fault. This
703 configuration is necessary to explain the consistent extensional deformation observed in western
704 Guatemala at >100,000 yr before present. In this model, the extending Caribbean plate was the
705 extending region within a dashpot between the end of the piston and the cylinder (Fig. 11). Over
706 geological time, extensional deformation has become progressively localized into the region

707 between the Guatemala City and Ipala grabens. The extensional strain associated with the triple
708 junction is being localized into the Guatemala City graben, as recorded by right-lateral slip on
709 the Jalpatagua fault and left-lateral slip on the Motagua fault. The mechanism for the
710 localization of extensional strain may be that western Guatemala is effectively pinned between
711 the North America and forearc slivers (also discussed in Alvarez-Gomez et al., 2019).

712 This “localizing dashpot” model differs from the Authemayou et al. (2011) zipper model
713 in two major ways. In our proposed model, the trailing edge of the Caribbean plate is
714 progressively abandoned, to become part of the forearc and/or the North American plate. In
715 contrast, the zipper model Authemayou et al. (2011) suggests that the entire Caribbean plate
716 escapes, which would result in the juxtaposition of the left-lateral Motagua-Polochic fault and
717 the right-lateral arc-parallel (e.g., Jalpatagua) fault. Alternatively, one could consider the
718 “localizing dashpot” model as a variant of the zipper model, if you allow that Caribbean material
719 can get stuck in the zipper. However, “localizing dashpot” model has more explanatory power,
720 because it also recognizes that the extensional structures in Honduras are also progressively
721 abandoned. Regardless, the “localizing dashpot” model provides a better description of the
722 recent history (~100 ka, at a minimum) and current motions associated of this triple junction. It
723 is possible that the zipper model of Authemayou et al. (2011) characterizes well the earlier
724 (Miocene?) deformation associated with this triple junction.

725

726 **6 Conclusions**

727 Analysis of minor faulting and four new $^{40}\text{Ar}/^{39}\text{Ar}$ dates in western Guatemala indicate
728 that internal deformation of the region was active in the Pliocene and part of the Quaternary,
729 recording roughly east-west elongation and slight transtension, but has ceased in an eastward

730 trend through time towards the Guatemala City graben. The geologic evidence supports that the
731 Guatemala City graben region is the current triple junction between the North America, forearc,
732 and Caribbean (NAFCA) plates.

733 The four analyzed outcrops all contain evidence of past faulting. $^{40}\text{Ar}/^{39}\text{Ar}$ dating and
734 unit correlation show that faulting within western Guatemala was active in the Pliocene (Nahuala
735 outcrop) and ceased in an eastward trend: by 84 ka at the westernmost outcrop Ilotenango, by 54
736 ka in the central Tecpan outcrop, and after 51 ka at the Xenacoj outcrop just west of the
737 Guatemala City graben, for which faulting on the main fault may still be active. Analysis of
738 minor faulting at these outcrops indicate E-W and ESE-directed elongation occurred at the
739 Tecpan and Ilotenango outcrops, in amounts of 0.64% and 15.8%, respectively. Additionally,
740 NE- and NNE-directed elongation was estimated at the Nahuala and Xenacoj outcrops, in
741 amounts of 4.2-4.7% and 11.5%, respectively.

742 We hypothesize that during the Pliocene and part of the Quaternary, the trailing wedge of
743 the Caribbean plate extended across Guatemala, between the Polochic-Motagua fault system and
744 the volcanic arc/forearc sliver. Further, this region underwent east-west elongation, and NE-
745 directed transtension, in a distributed fashion across minor and major faults and structures.
746 Elongation ceased on normal faults in western Guatemala as deformation became localized in the
747 Guatemala City graben and surrounding structures. The same effect occurred in Honduras
748 adjacent to the Motagua fault, as normal faults no longer accommodate any of the geodetic
749 movement in that region (Ellis et al., 2019). We propose a “localizing dashpot” model, in which
750 the Caribbean plate is pulled out from between North American and the forearc plates. The
751 extensional strain localization into the Guatemala City graben progressively transferred western
752 Guatemala to the forearc and/or North America plate. This model of time-progressive strain

753 localization or “localizing dashpot” agrees with past deformation observed in western Guatemala
754 and western Honduras and the current GPS velocity model which depicts a North America-
755 forearc and Caribbean plate boundary that ends at the Guatemala City graben.

756

757 **Acknowledgements**

758 This work was funded by the National Science Foundation [grant EAR-1144418
759 (DeMets)]. We thank Guatemalan institutions that provided technical and safety support
760 including University of Guatemala in Coban, INSIVUMEH of Guatemala, and CONRED of
761 Guatemala. Special thanks go to Joshua Rodenas, Roberto Mérida Boogher, Carlos Pérez, and
762 Victor Pérez, who aided in field work, Sergio Mendez Rojas, Allen Schaen, Bryan Wathen, and
763 Randy Williams, who aided in lab work, and Neal Lord, who was instrumental in the geodetic
764 operations and field work. Geochemical, geochronological, and geodetic datasets for this
765 research are described in this paper and the supplemental material: [Garnier et al., in review].
766 Datasets containing individual fault measurements are described in this PhD dissertation:
767 [Garnier, 2020; University of Wisconsin-Madison]. Original rock samples used in the
768 geochemical and geochronological analyzes supporting this research are available in the geology
769 museum collections at the University of Wisconsin-Madison.

770

771 **Supplemental Material**

772 Appendix A.1 Table of GPS site velocities and site information.

773 Appendix A.2 Complete $^{40}\text{Ar}/^{39}\text{Ar}$ data table for west Guatemala samples.

774 Appendix A.3 Additional details from the Santa Domingo Xenacoj outcrop.

775

776 **References**

- 777 Alvarado, D., DeMets, C., Tikoff, B., Hernandez, D., Wawrzyniec, T.F., Pullinger, et al., 2011,
778 Forearc motion and deformation between El Salvador and Nicaragua: GPS, seismic,
779 structural, and paleomagnetic observation: *Lithosphere*, v. 3, no. 1, p. 3-21, doi:
780 10.1130/L108.1.
- 781 Alvarado Cabrera, G. D., and Herrer Ibáñez, I. R., 2001. Mapa Fisiográfico-Geomorfológico de
782 la República de Guatemala a escala 1:250,000: Ministerio de Agricultura, Ganadería y
783 Alimentación.
- 784 Álvarez-Gómez, J. A., Meijer, P. T., Martínez-Díaz, J. J., and Capote, R., 2008, Constraints from
785 finite element modeling on the active tectonics of northern Central America and the
786 Middle America Trench: *Tectonics*, v. 27, p. TC1008, doi:10.1029/2007TC002162.
- 787 Álvarez-Gómez, J. A., Staller Vázquez, A., Martínez-Díaz, J. J., Canora, C., Alonso-Henar, J.,
788 Unsua-Arévalo, J. M., and Béjar-Pizarro, M., 2019, Push-pull driving of the Central
789 America Forearc in the context of the Cocos-Caribbean-North America triple junction:
790 *Nature*, v. 9, 11164.
- 791 Andreani, L. and Gloaguen, R., 2016, Geomorphic analysis of transient landscapes in the Sierra
792 Madre de Chiapas and Maya Mountains (northern Central America): implications for the
793 North American-Caribbean-Cocos plate boundary: *Earth Surface Dynamics*, v. 4, p. 71-
794 102.
- 795 Authemayou, C., Brocard, G., Teyssier, C., Simon-Labric, T., Guittierrez, A., Chiquin, E.N., et
796 al., 2011, The Caribbean-North America-Cocos triple junction and the dynamics of the
797 Polochic-Motagua fault systems: Pull-up and zipper models: *Tectonics*, v. 30, p. TC3010,
798 doi:10.1029/2010TC002814.
- 799 Authemayou, C., Brocard, G., Teyssier, C., Suski, B., Consenza, B., Morán-Ical, S., et al., 2012,
800 Quaternary seismo-tectonic activity of the Polochic Fault, Guatemala: *Journal of*
801 *Geophysical Research*, v. 117, p. B07403.
- 802 Borchardt, G. A. and Harward, M. E., 1971, Trace Element Correlation of Volcanic Ash Soils:
803 *Soil Science Society of America Proceedings*, v. 35, p. 626-631.
- 804 Burkart, B. and Self, S., 1985, Extension and rotation of crustal blocks in northern Central
805 America and effect on the volcanic arc: *Geology*, v. 13, p. 22-26.
- 806 Burkart, B., 1978, Offset across the Polochic fault of Guatemala and Chiapas, Mexico: *Geology*,
807 v. 6, p. 328-332.
- 808 Burkart, B., 1983, Neogene North American-Caribbean Plate boundary across northern Central
809 America: Along the Polochic fault: *Tectonophysics*, v. 99, p. 251-270.
- 810 Clohan, G. M. and Reynolds, J. C., 1977, The Geology of the Eastern Portion of the Sololá
811 Quadrangle, Guatemala (Undergraduate thesis): Dartmouth College, 72 p.
- 812 Correa-Mora, F., DeMets, C., Alvarado, D., Turner, H.L., Mattioli, G.S., Hernandez, D., et al.,
813 2009, GPS-derived coupling estimates for the Central America subduction zone and
814 volcanic arc faults: El Salvador, Honduras, and Nicaragua: *Geophysical Journal*
815 *International*, v. 179, p. 1279-1291.
- 816 Cronin, V. S., 1992, Types and kinematic stability of triple junctions: *Tectonophysics*, v. 207, p.
817 287-301.
- 818 DeMets, C., 2001, A new estimate for present-day Cocos-Caribbean plate motion: Implications
819 for slip along the Central American volcanic arc: *Geophysical Research Letters*, v. 28,
820 no. 21, p. 4043-4046.

821 Drexler, J. W., Rose, W. I., Sparks, R. S. J., and Ledbetter, M. T., 1980, The Los Chocoyos Ash,
822 Guatemala: A Major Stratigraphic Marker in Middle America and in Three Oceans
823 Basins: Quaternary Research, v. 13, p. 327-345.

824 Eggert, R. G. and Lea, P. D., 1978, The Geology of the Central Portion of the Santa Catarina
825 Ixtahuacan Quadrangle, Guatemala (Undergraduate thesis): Dartmouth College, 86 p.

826 Ellis, A., DeMets, C., Briole, P., Cosenza, B., Flores, O., Graham, S. E., et al., 2018, GPS
827 constraints on deformation in northern Central America from 1999 to 2017, Part 1 –
828 Time-dependent modelling of large regional earthquakes and their post-seismic effects:
829 Geophysical Journal International, v. 214, p. 2177-2194.

830 Ellis, A.P., DeMets, C., Briole, P., Cosenza, B., Flores, O., Graham, S. E., et al.,
831 2019, Deformation in northern Central America from 1999 to 2017 using GPS
832 observations, Part 2: Block rotations, fault slip rates, fault locking, and distributed
833 deformation: Geophysical Journal International, v. 218, p. 729-754.

834 Franco, A., Lasserre, C., Lyon-Caen, H., Kostoglodov, V., Molina, E., Guzman-Speziale, M., et
835 al., 2012, Fault kinematics in northern Central America and coupling along the
836 subduction interface of the Cocos Plate, from GPS data in Chiapas (Mexico), Guatemala
837 and El Salvador: Geophysical Journal International, v. 189, p. 1223-1236.

838 Garibaldi, N., Tikoff, B. & Hernández, W., 2016, Neotectonic deformation within an extensional
839 stepover in El Salvador magmatic arc, Central America: Implication for the interaction of
840 arc magmatism and deformation: Tectonophysics, v. 693, p. 327-339.

841 Garnier, B., Tikoff, B., Flores, O., Jicha, B., DeMets, C., Cosenza-Murales, B., Hernandez, D.,
842 Marroquin, G., Mixco, L., and Hernandez, W., 2020, An integrated structural and GPS
843 study of the Jalpatagua Fault, southeastern Guatemala: submitted to Geosphere.

844 Gordon, M. and Muehlberger, W. R., 1994, Rotation of the Chortís block causes dextral slip on
845 the Guayupe fault: Tectonics, v. 13, no. 4, p. 858-872.

846 Gross, M. R. and Engelder, T., 1999, Strain accommodated by brittle failure in adjacent units of
847 the Monterey Formation, U.S.A.: scale effects and evidence for uniform displacement
848 boundary conditions: Journal of Structural Geology, v. 17, no. 9, p. 1303-1318.

849 Guzman-Speziale, M., Pennington, W. D., and Matumoto, T., 1989, The triple junction of the
850 North America, Cocos, and Caribbean plates: Seismicity and Tectonics: Tectonics, v. 8,
851 no. 5, p. 981-997.

852 Holekamp, C.P., Larson, J.E., and Lundstrom, S.C., 1978, The geology of the adjoining portions
853 of the Santa Catarina Ixtahuacán and Sololá quadrangles, Guatemala (Undergraduate
854 thesis): Dartmouth College, 47 p.

855 Hughes, J.M., 1978, Geology and Petrology of Caldera Tzanjuyub, Western Guatemala (MS
856 thesis): Dartmouth College, 129 p.

857 Jicha, B.R., Singer, B.S., and Sobol, P., 2016, Re-evaluation of the ages of $^{40}\text{Ar}/^{39}\text{Ar}$ sanidine
858 standards and supereruptions in the western U.S. using a Noblesse multi-collector mass
859 spectrometer, Chemical Geology, v. 431, p. 54-66.

860 Koch, A. J., 1970, Stratigraphy, petrology, and distribution of Quaternary pumice deposits of the
861 San Cristobal group, Guatemala City Area, Guatemala [Ph.D. thesis]: University of
862 Washington.

863 Koch, A. J. and McLean, H., 1975, Pleistocene and Tephra and Ash-Flow Deposits in the
864 Volcanic Highlands of Guatemala: GSA Bulletin, v. 86, p. 529-541.

865 Lyon-Caen, H., Barrier, E., Lasserre, C., Franco, A., Arzu, I., Chiquin, L., et al., 2006,
866 Kinematics of the North America-Caribbean-Cocos plates in Central America from new

867 GPS measurements across the Polochic-Motagua fault system: Geophysical Research
868 Letters, v. 33, p. L19309.

869 Marrett, R. and Allmendinger, R. W., 1991, Estimates of strain due to brittle faulting: sampling
870 of fault populations: Journal of Structural Geology, v. 13, no. 6, p. 735-738.

871 Marrett, R. and Allmendinger, R. W., 1992, Amount of extension on “small” faults: An example
872 from the Viking graben: Geology, v. 20, p. 47-50.

873 McKenzie, D. P. & Morgan, W. J., 1969, Evolution of Triple Junctions: Nature, v. 224, p. 125-
874 133.

875 McLean, H., 1970, Stratigraphy, mineralogy, and distribution of the Sumpango group pumice
876 deposits in the volcanic highlands of Guatemala [Ph.D. thesis]: University of
877 Washington, 99 p.

878 Morgan, W.J., 1968, Rises, trenches, great faults, and crustal blocks: Journal of Geophysical
879 Research, v. 73, no. 6, p. 1959-1982.

880 Muehlberger, W.R. and Ritchie, A.W., 1975, Caribbean-Americas plate boundary in Guatemala
881 and southern Mexico as seen on Skylab IV orbital photography: Geology, v. 3, p. 232-
882 235.

883 Newhall, C. G., 1987, Geology of the Lake Atitlán Region, western Guatemala: Journal of
884 Volcanology and Geothermal Research, v. 33, p. 23-55.

885 Phipps Morgan, J.P., Ranero, C.R., and Vannucchi, P., 2008, Intra-arc extension in Central
886 America: Links between plate motions, tectonics, volcanism, and geochemistry: Earth
887 Planetary Science Letters, v. 272, p. 365-371.

888 Plafker, G., 1976, Tectonic Aspects of the Guatemala Earthquake of 4 February 1976: Science,
889 v. 193, no. 4259, p. 1202-1208.

890 Reynolds, J. H., 1977, Tertiary Volcanic Stratigraphy of Northern Central America [Masters
891 thesis]: Dartmouth College.

892 Reynolds, J. H., 1980, Late Tertiary Volcanic Stratigraphy of Northern Central America:
893 Bulletin of Volcanology, v. 43, no. 3, p. 601-607.

894 Ritchie, A. W., 1975, Geology of the San Juan Sacatepéquez Quadrangle, Guatemala, Central
895 America (Ph.d dissertation): University of Texas at Austin, 132p.

896 Rogers, R.D., Karason, H., and van der Hilst, R.D., 2002, Epeirogenic uplift above a detached
897 slab in northern Central America: Geology, v. 30, no. 11, p. 1031-1034.

898 Rogers, R. D. and Mann, P., 2007, Transtensional deformation of the western Caribbean-North
899 America plate boundary zone: The Geological Society of America Special Paper, v. 428,
900 p. 37-64.

901 Rose, W. I., Newhall, C. G., Bornhorst, T. J., and Self, S., 1987, Quaternary Silicic Pyroclastic
902 deposits of Atitlan Caldera, Guatemala: Journal of Volcanology and Geothermal
903 Research, v. 33, p. 57-80.

904 Rose, W. I., Grant, N. K., and Easter, J., 1979, Geochemistry of the Los Chocoyos Ash,
905 Quezaltenango Valley, Guatemala: Geological Society of America Special Paper, v. 180,
906 p. 87-99.

907 Rose, W. I., Conway, F. M., Pullinger, C. R., Deino, A., and McIntosh, W. C., 1999, An
908 improved age framework for late Quaternary silicic eruptions in northern Central
909 America: Bulletin of Volcanology, v. 61, p. 106-120.

910 Rose, W. I., Hahn, G. A., Drexler, J. W., Malinconico, M. L., Peterson, P. S., and Wunderman,
911 R. L., 1981, Quaternary Tephra of Northern Central America, *in* Self, S., Sparks, R.S.J.,

912 eds., *Tephra Studies*: Springer, Dordrecht, NATO Advanced Study Institutes Series
913 (Series C – Mathematical and Physical Sciences), v. 75, p. 193-211.

914 Sarna-Wojcicki, A. M., Bowman, H. R., Meyer, C. E., Russell, P. C., Woodward, M. J., McCoy,
915 G., et al., 1984, Chemical analyses, correlations, and ages of upper Pliocene and
916 Pleistocene ash layers of East-Central and Southern California: Geological Survey
917 Professional Paper, v. 1293, 22 p.

918 Sarna-Wojcicki, A., 2000, Tephrochronology, *in* Noller, J. S., Sowers, J. M., and Lettis, W. R.,
919 eds., *Quaternary Geochronology: Methods and Applications*: Washington, DC, American
920 Geophysical Union, AGU Reference Shelf Series, v. 4, p. 357-377.

921 Schindlbeck, J. C., Kutterolf, S., Freundt, A., Eisele, S., Wang, K.-L., and Frische, M., 2016,
922 Miocene to Holocene Marine Tephrostratigraphy Offshore Northern Central America and
923 Southern Mexico: Pulsed Activity of known Volcanic Complexes: *Geochemistry,*
924 *Geophysics, Geosystems*, v. 19, p. 4143-4173.

925 Titus, S. J., Housen, B., and Tikoff, B., 2007, A kinematic model for the Rinconada fault system
926 in central California based on structural analysis of en echelon folds and paleomagnetism:
927 *Journal of Structural Geology*, v. 29, p. 961-982.

928 Walsh, J., Watterson, J., and Yielding, G., 1991, The importance of small-scale faulting in
929 regional extension: *Nature*, v. 351, p. 391-393.

930 Weyl, R., 1980, *Geology of Central America*: Berlin, Borntraeger, 371 p.

931 Williams, H., 1960, Volcanic history of the Guatemalan Highlands: University of California
932 publications in Geological Sciences, v. 38, p. 1-86.

933 Wunderman, R. L., and Rose, W. I., 1984, Amatitlan, an actively resurging cauldron 10 km
934 south of Guatemala City: *Journal of Geophysical Research*, v. 89, no. B10, p. 8525-8539.

935 Xu, S.S., Velasquillo-Martínez, L.G., Grajales-Nichimura, J.M., Murillo-Muñetón, G., and
936 Nieto-Samaniego, A.F., 2007, Methods for quantitatively determining fault slip using
937 fault separation: *Journal of Structural Geology*, v. 29, p. 1709-1720.

938 Xu, S.S., Nieto-Samaniego, A.F., and Alaniz-Alvarez, S.A., 2009, Quantification of true
939 displacement using apparent displacement along an arbitrary line on a fault plane:
940 *Tectonophysics*, v. 467, p. 107-118.

941 York, D., 1973, Evolution of Triple Junctions: *Nature*, v. 244, p. 341-342.

942
943

944 **Tables**

945

946 Table 1. DESCRIPTIONS OF COLLECTED SAMPLES

Sample	Unit description	Mineralogy (including results from mineral count analysis)	Present structures	Age	Interpretation
WH19S5	Three thin felsic tephra (1.15 m, 1.17 m, and 1.3 m thicknesses) separated by paleosols. Each tephra contains pumice fragments and ash matrix		Unfaulted	<51 ka	Possibly I tephra from Amatitlan caldera
17JF56J & WH19S6 Xenacoj	White pumice-rich tephra containing pumice fragments, phenocrysts, and ash.	Pumice (up to 1.5 cm long) contains 4% mafic phenocrysts, 8% felsic phenocrysts, and 88% glass fragments. Mafic phenocrysts are biotite, hornblende, with 20% being magnetite.	Unfaulted	51 ka (Schindlbeck et al., 2016)	E tephra

17JF56R Xenacoj	Thick, white and grey tephra containing pumice fragments, phenocrysts, and ash. Pumice vesicles have the linear, spindle shape.	Pumice (1-3 cm long) contains up to 2% mafic phenocrysts, 3-4% felsic phenocrysts, and 94-97% glass fragments. Mafic phenocrysts are mostly biotite with a few grains of magnetite.	Faulted, NW-striking normal faults	1.145 ± 0.061 Ma (WiscAr lab, 2018)	
17JF56A Xenacoj	Tan vitric tuff containing phenocrysts and glass fragments.	Tuff contains 14% mafic phenocrysts (dominantly biotite with lesser amounts of hornblende and magnetite), 30-37% felsic phenocrysts, and 46-53% glass fragments.	Faulted, NW-striking normal faults	1.495 ± 0.057 Ma (WiscAr lab, 2018)	
17JF56S Xenacoj	Massive grey volcanic deposit, highly unsorted, containing large bombs of andesite porphyry, phenocrysts, and ash. Glass fragments are either light-gray colored with thin-walled, linear vesicles or dark gray colored with thick-walled, round vesicles.	Andesite porphyry blocks (Sample 17JF56S): Biotite, hornblende, and feldspar phenocrysts in a grey aphanitic matrix. Ash matrix (Sample 17JF56K) contains 2-3% biotite phenocrysts, 8-16% felsic phenocrysts, and 61-68% glass fragments.	Faulted, NW-striking normal faults	9.117 ± 0.006 Ma (WiscAr lab, 2018)	Biotite-rich crystal vitric tuff
WH19S9 Tecpan	Upper tephra containing angular pumice fragments, little sorted, reverse grading, and few lithics (1-1.5%).		Unfaulted	<51 ka	Possibly I tephra from the Atitlan caldera
WH19S8 Tecpan	Middle tephra of white and yellow pumice, well sorted, slight reverse gradation, 1-2% fine lithics, and golden biotite (2%) and hornblende (1%) phenocrysts. Pumice fragments have very fine vesicles.		Unfaulted	51 ka	E tephra
WH19S7 Tecpan	Lower tephra, ~1 m thick, contains pumice fragments and 5-7% of basaltic lithics. Pumice fragments are light and grey in color and somewhat sorted. Horizons of irregular brown, oxidized layers up to 3 cm thick. Paleosol overlies tephra.		Unfaulted	54 ka	C tephra
14GM5b Tecpan	Thick, red, reworked deposits of the Los Chocoyos. Rounded cobbles of various mafic lithologies, poorly sorted, in a clay-rich red/tan matrix.		Faulted, N-S and NE-striking normal faults	Post-Los Chocoyos	Los Chocoyos sediments
14GM14 M Nahuala	Green-ish grey extrusive basalt/andesite flow with foliation created by linear bands of light-colored minerals.	Aphanitic mafic matrix with thin, linear, parallel and anastomosing, olivine bands.	Unfaulted	3.227 ± 0.033 Ma (WiscAr lab, 2018)	Tertiary Cerro Jox basalt/andesite flow
14GM14k Nahuala	2-3 thin white tephra layers, interlayered with soil horizons		Unfaulted	<51 ka	Likely I tephra from Atitlan caldera

Faulted Lithology Nahuala	Grey and white, indurated, lithic-rich lahar/mudflow deposit. Deposits contain rounded pebbles of andesite/basalt, broken felsic phenocrysts, in a grey, sandy matrix.		Faulted, NW-striking normal faults	Pliocene	Tertiary Lahars and mudflows
14GM7 Ilotenango	>40m thick, white, pumice-rich lapilli tephra. Very linear, spindle-shaped vesicles in pumice. Carbonized logs	Pumice (3-7 cm long) contains 96% glass, 4% felsic phenocrysts, and <1% mafic phenocrysts, nearly all of which are biotite.	Unfaulted	84 ka (Dexler et al., 1980)	Los Chocoyos tephra
14GM8 Ilotenango	Highly indurated tan reworked volcanic deposit with some visible layering and iron-stained bands. Possible lahar deposit based on unsorted and well indurated nature.		Faulted, NE-striking normal faults	Middle to Upper Miocene	Tertiary reworked deposit (Chalatenango or Balsamo Fm)

947
948
949

Table 2. MINOR FAULT ANALYSIS RESULTS

Location	Lf (m)	Max Elongation	# of Faults	dF (m)	Elongation (%)	he (m)	dFr (m)	Revised elongation (%)
West of Guatemala City graben								
<i>Xenacoj</i> 1a	86.8	33	44	1.49	1.7	0.123	1.76	2.1
<i>Xenacoj</i> 1b	78.5	34	23	8	11.3	0.086	8.1	11.5
<i>Tecpan</i> 2	212.6	83	10	0.83	0.4	0.52	1.34	0.64
<i>Nahuala</i> 3	166.4	56	13	6.3	3.9	.42-1.1	6.7-7.4	4.2-4.7
<i>Ilotenango</i> 4	98.3	112	25	8.34	9.3	5.08	13.42	15.8

950
951
952
953

Table 3A. XRF DATA FROM COLLECTED SAMPLES WITHIN THE WESTERN GUATEMALA WEDGE

Sample Id	17JF56S	17JF56A	17JF56R	WH19S6	WH19S5	WH19S7	WH19S8	WH19S9
Location	Xenacoj			Tecpan				
Latitude	14.69			14.72				
Longitude	-90.70			-91.96				
Normalized Major Elements (Weight %):								
SiO ₂	74.43	69.72	74.27	70.72	68.56	68.10	72.89	76.01
TiO ₂	0.345	0.370	0.236	0.435	0.411	0.422	0.349	0.136
Al ₂ O ₃	14.31	17.37	16.49	16.73	19.45	17.62	14.72	14.28
FeO*	1.80	3.06	1.70	2.37	3.42	3.97	2.20	0.86
MnO	0.035	0.067	0.062	0.101	0.140	0.135	0.091	0.073
MgO	0.32	0.75	0.20	0.54	0.71	1.10	0.55	0.17
CaO	0.61	2.35	0.85	1.45	2.32	3.04	1.42	0.82
Na ₂ O	3.23	3.22	2.39	3.77	3.11	3.65	3.65	3.36
K ₂ O	4.92	3.08	3.78	3.83	1.81	1.89	4.11	4.27
P ₂ O ₅	0.005	0.016	0.020	0.067	0.063	0.077	0.023	0.021
Total	100.00	100.00	100.00	100.00	100.00	100.00	100.00	100.00

Trace Elements (ppm):								
Ni	6	5	4	4	3	3	3	3
Cr	3	3	3	3	2	3	3	5
Sc	3	8	4	5	6	6	4	3
V	16	45	18	19	28	52	24	7
Ba	810	885	988	1149	1016	861	1045	1019
Rb	217	89	98	102	42	48	117	118
Sr	76	260	97	193	306	351	152	115
Zr	236	130	104	289	189	142	247	66
Y	23	19	17	27	20	14	20	11
Nb	14.4	5.5	6.9	7.6	4.2	3.3	6.5	5.6
Ga	17	16	14	17	18	17	14	13
Cu	1	9	7	7	9	17	6	6
Zn	49	44	31	54	69	66	47	25
Pb	20	13	14	16	12	9	15	14
La	37	28	22	25	20	12	19	19
Ce	52	39	38	48	36	24	41	35
Th	15	9	10	8	4	3	8	12
Nd	24	20	17	24	18	14	14	12
U	5	3	4	3	2	1	4	4

954

955

Table 3A. Continued

Sample Id	14GM14k	14GM7
Location	Nahuala	Ilotenango
Latitude	14.82	15.04
Longitude	-91.35	-91.23

Normalized Major Elements (Weight %):

SiO ₂	67.35	77.37
TiO ₂	0.454	0.110
Al ₂ O ₃	18.18	12.97
FeO*	3.42	0.66
MnO	0.106	0.067
MgO	0.84	0.12
CaO	3.20	0.81
Na ₂ O	3.68	3.64
K ₂ O	2.66	4.24
P ₂ O ₅	0.117	0.014
Total	100.00	100.00

Trace Elements (ppm):

Ni	5	3
Cr	3	2
Sc	8	2
V	52	2
Ba	892	1012
Rb	92	122
Sr	378	102
Zr	190	61
Y	17	11

Nb	6.6	6.0
Ga	19	13
Cu	10	2
Zn	75	24
Pb	22	14
La	24	20
Ce	39	34
Th	8	12
Nd	17	13
U	2	3

956
957
958
959

Table 3B. XRF SIMILARITY COEFFICIENT BETWEEN COLLECTED SAMPLES AND QUATERNARY TEPHRAS

	14GM7	14GM14k	WH19S7	WH19S8	WH19S9	17JF56J	WH19S6	WH19S5
I falls	0.57	0.82*	0.77	0.80	0.62	0.73	0.81	0.85*
E	0.58	0.75	0.69	0.85*	0.62	0.75	0.91*	0.76
C	0.49	0.90*	0.84*	0.66	0.52	0.68	0.73	0.81*
H flow low K average	0.63	0.71	0.69	0.75	0.66	0.66	0.76	0.74
H flow high K average	0.91*	0.50	0.47	0.71	0.92	0.55	0.61	0.51
H fall average	0.87*	0.54	0.51	0.73	0.89	0.58	0.64	0.54
Tflow	0.61	0.70	0.64	0.86	0.66	0.77	0.90	0.71
Tt fall	0.62	0.70	0.64	0.87	0.67	0.77	0.90	0.71
Z5	0.57	0.73	0.67	0.82	0.61	0.78	0.93	0.75
Z4	0.56	0.76	0.70	0.82	0.60	0.78	0.91	0.76
Z2	0.47	0.82	0.86	0.63	0.49	0.63	0.68	0.81
W flow average	0.67	0.65	0.62	0.80	0.72	0.67	0.76	0.64
W fall average	0.64	0.71	0.68	0.78	0.67	0.70	0.78	0.73
Lf(2)	0.56	0.73	0.67	0.80	0.60	0.79	0.89	0.73
Lf(1)	0.53	0.76	0.69	0.73	0.56	0.75	0.84	0.74
Lt	0.59	0.71	0.64	0.84	0.63	0.80	0.91	0.71

960 **bold*** coefficients are the highest values for a given sample

961
962

Table 4. RESULTS OF $^{40}\text{Ar}/^{39}\text{Ar}$ ANALYSIS

Sample #	Location	Wt. % SiO ₂	Latitude (N)	Longitude (W)	Material	$^{40}\text{Ar}/^{36}\text{Ar}_i \pm 2s$	Isochron age (Ma) $\pm 2s$	N	^{39}Ar %	MSWD	Plateau age (Ma) $\pm 2s$
17JF56R	Xenacoj	74.3	14.6943	90.6968		\pm	\pm	6 of 8	1.20	1.145	± 0.061
17JF56A	Xenacoj	69.7	14.6943	90.6968	Plagioclase	\pm	\pm	3 of 7	0.05	1.495	± 0.057
17JF56S	Xenacoj	74.4	14.6948	90.6962			\pm	16 of 17	1.40	9.115	± 0.008
14GM14	Nahuala	67.4	14.8215	91.3472							

963

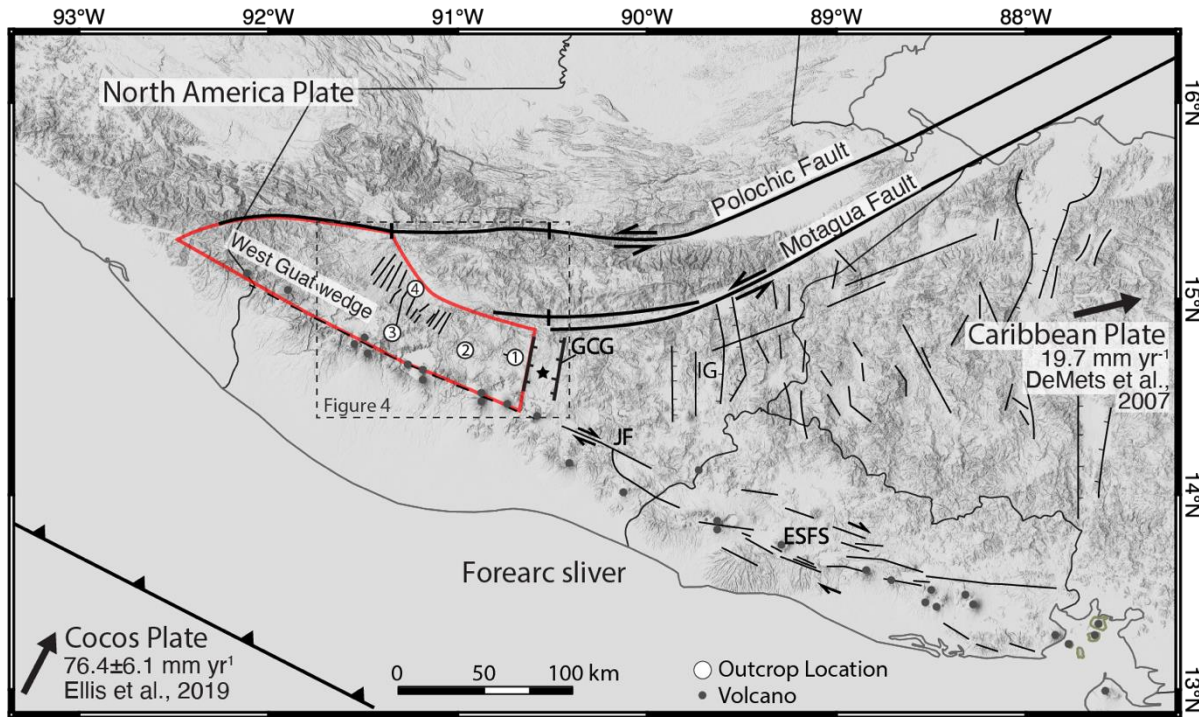
964
965

Table 5. ESTIMATED ELONGATION RATES FOR FAULTED OUTCROPS

Outcrop	Length added (dFr from Table 2, mm)	Upper limit of fault timing (age of unfaulted deposit)		Lower limit of fault timing (age of youngest faulted deposit)		Time span	Strain rate (mm yr ⁻¹)
		Deposit	Age	Deposit	Age		
Xenacoj 1a	176						<0.0002
Xenacoj 1b	810	E tephra, youngest unfaulted deposit	51 ka	Faulted grey tuff, sample 17JF56R	1.145±0.061 Ma	1.1 Ma	<0.01
Tecpan	134	C tephra	54 Ka	Los Chocoyos	84 ka	30 ka	0.045
Nahuala	670-740	Cerro Jox basalt/andesite flow	3.2 Ma	Balsamo Formation (Late Miocene boundary)	11.14 Ma	7.94 Ma	<0.001
Ilotenango	1342	Los Chocoyos	84± 5 ka	Balsamo or Chalatenango formations	2.58 Ma or 5.33 Ma	1.74-5.2 Ma	0.0003-0.0008
Ilotenango (extrapolated area)	632000	Los Chocoyos	84± 5 ka	Balsamo or Chalatenango formations	2.58 Ma or 5.33 Ma	1.74-5.2 Ma	1.2-3.6

966
967
968

Figures

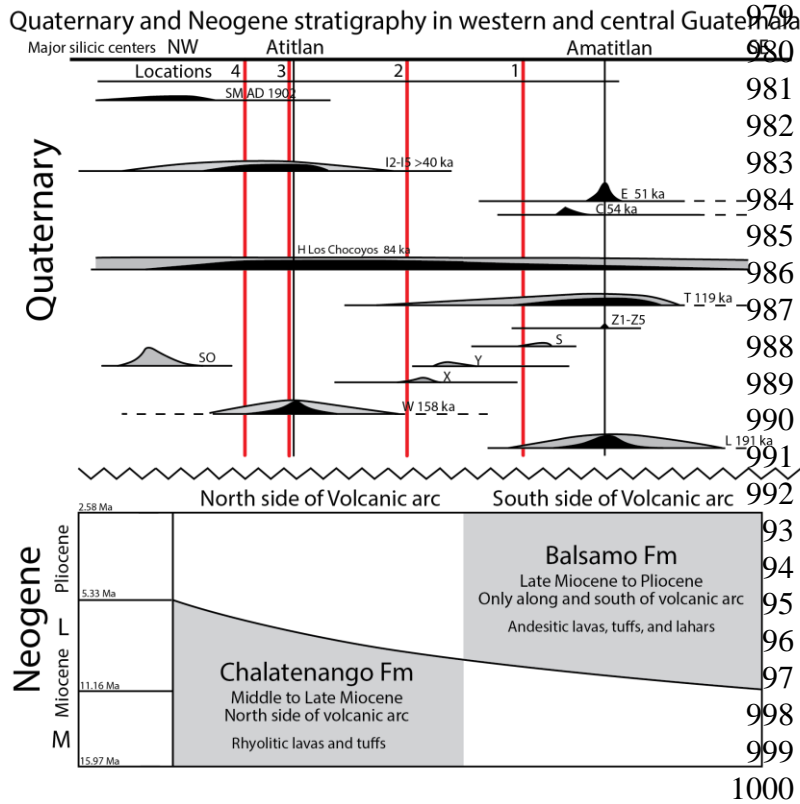


969
970
971
972
973
974

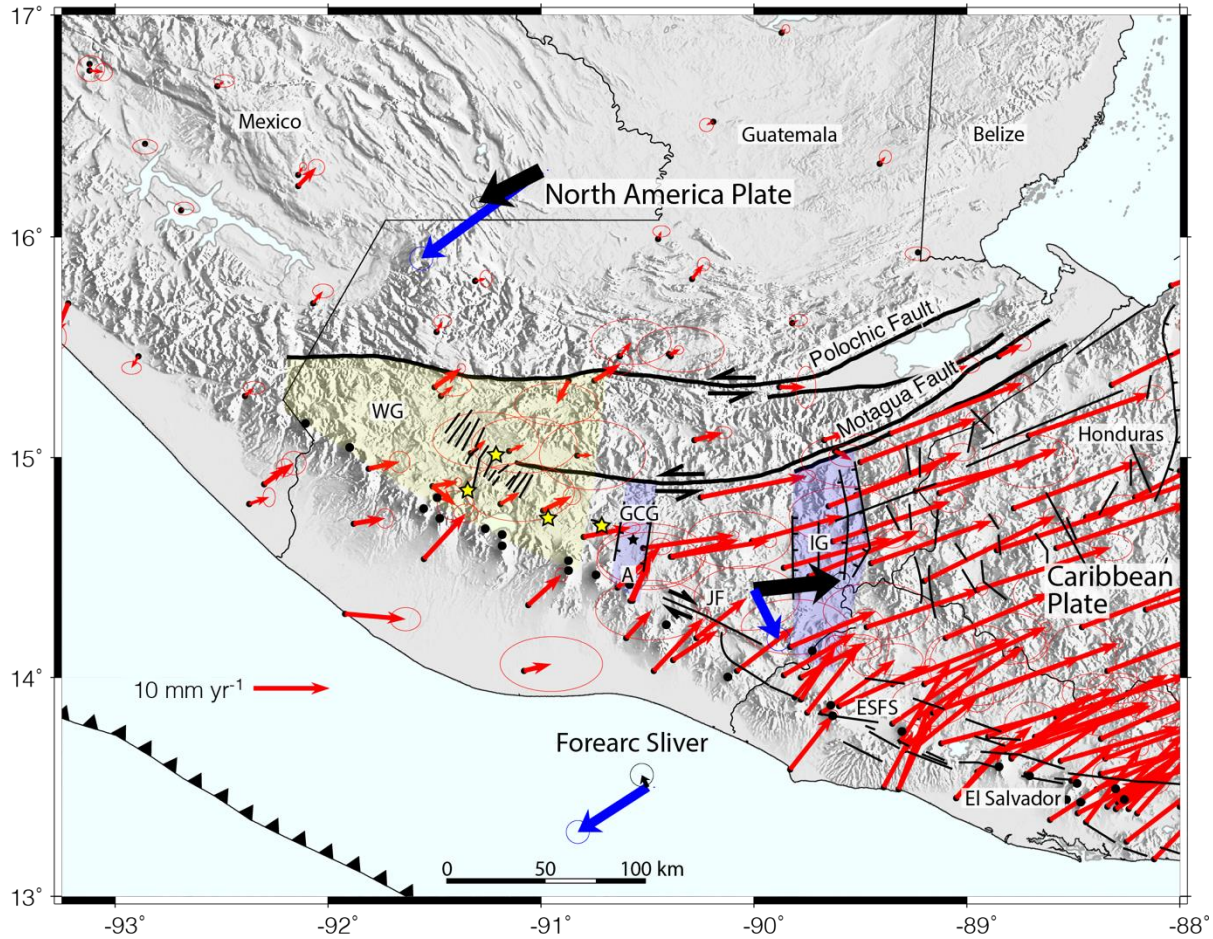
Figure 1. Annotated DEM of North America, Caribbean, and Cocos plate interactions in north Central America. The major structures are identified, along with the Guatemala City graben (GCG) containing Guatemala City (star), the Ipala graben (IG), the Jalpatagua fault (JF), and the El Salvador fault system (ESFS). Mapped faults in Honduras are from Rogers, 2002. The west Guatemalan wedge is outlined in red, with the Polochic fault, Guatemala City graben, and the

975 volcanic arc as the major bounding structures. Gray dashed box outlines the area presented in
 976 Figure 4.

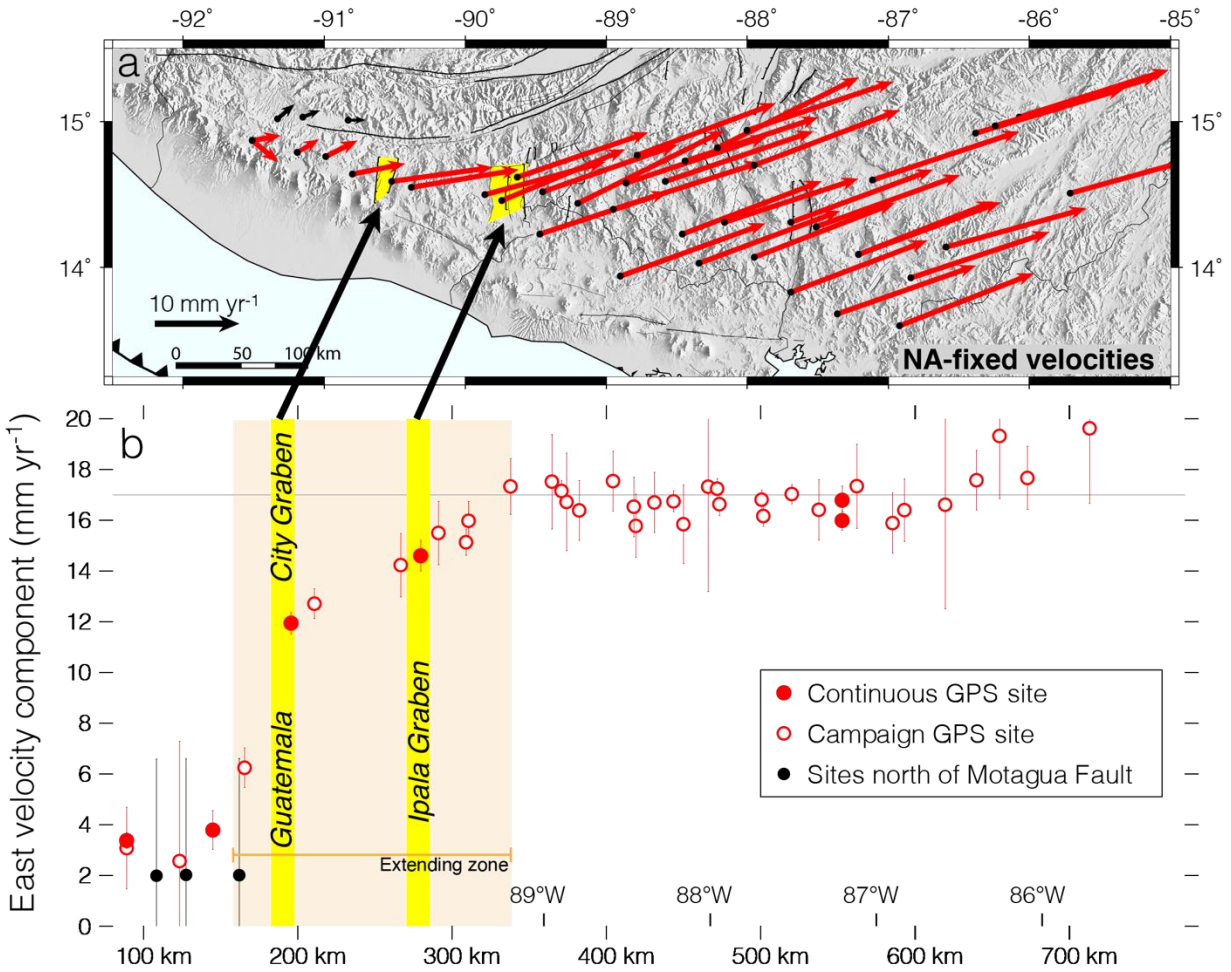
977
 978



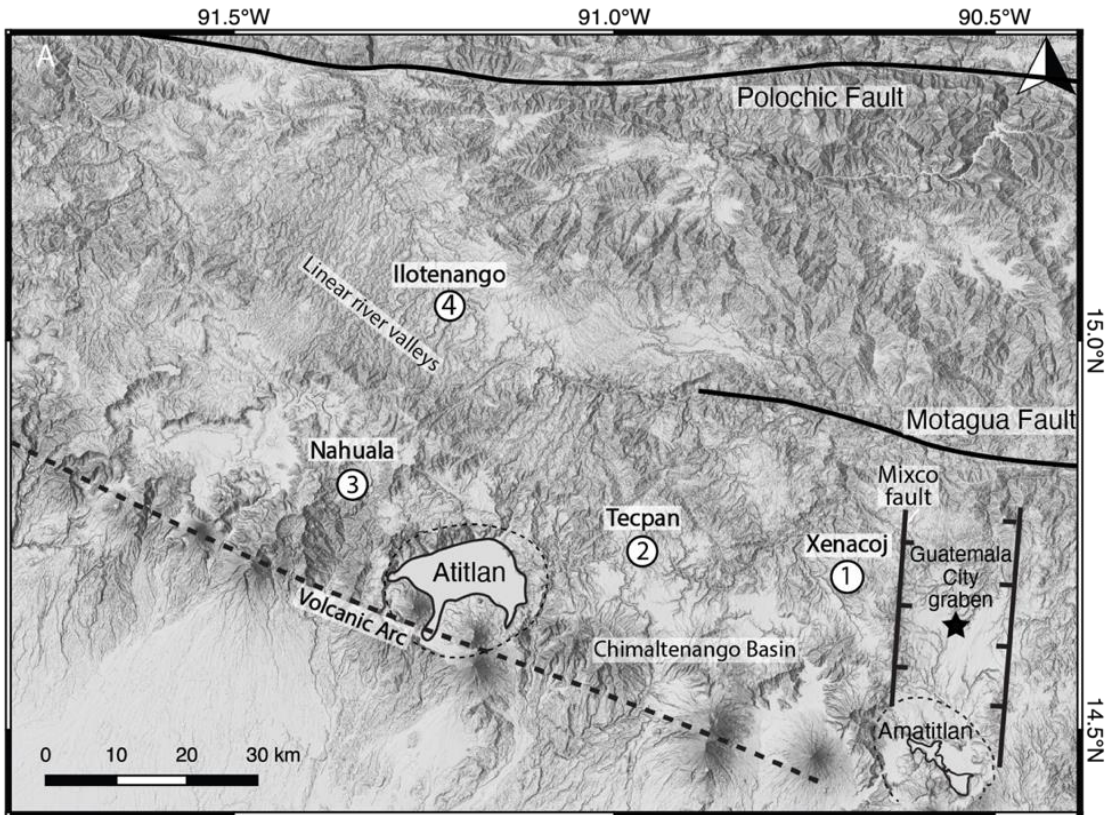
1001 Figure 2. Quaternary and Neogene stratigraphy of southwestern and southcentral Guatemala.
 1002 Top portion describes the Quaternary stratigraphy (modified from Rose et al., 1999), with
 1003 vertical red lines indicating the location of outcrops in relation to the major rhyolitic centers.
 1004 Bottom portion describes the Neogene stratigraphy.



1005
 1006 Figure 3A. Observed GPS site velocities relative to a stationary North America plate (red
 1007 arrows), corrected for elastic deformation attributed to locked faults in the study area. The
 1008 velocities in the figure are from Appendix A.1 in the supplemental material. Elastic deformation
 1009 at each site is estimated with the TDEFNODE model described in Ellis et al. (2018, 2019). Bold
 1010 black and blue arrows show absolute velocities of the North America and Caribbean plates and
 1011 Central America forearc sliver in mantle-fixed (Wang et al., 2018) and no-net-rotation (Argus et
 1012 al., 2010) frames of reference. Ellipses show the 1-sigma uncertainties. Abbreviated features:
 1013 WG = Western Guatemala; GCG = Guatemala City graben (black star- Guatemala City); A =
 1014 Amatitlan caldera; JF = Jalpatagua fault; IG = Ipala graben; ESFS = El Salvador fault system.
 1015 Yellow stars represent faulted outcrops used in minor fault analysis.

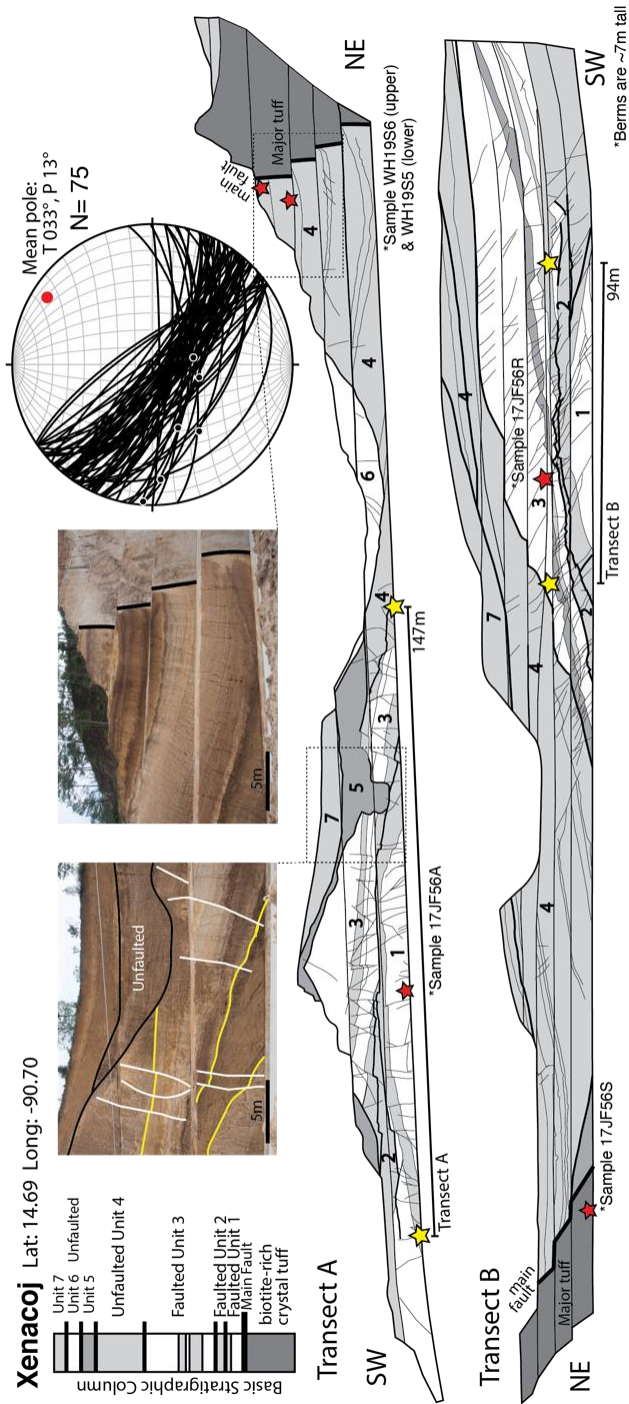


1016
 1017 Figure 3B. a. East-to-west transect of measured GPS site velocities relative to the North
 1018 America plate. Each measured velocity is corrected for an interseismic elastic velocity
 1019 component due to the locked faults in our best-fitting elastic block model. b. East velocity
 1020 components for sites from Panel A versus west-to-east distance across the transect. Filled and
 1021 open red circles show continuous and campaign site rates, respectively. The rates indicated by
 1022 the black circles show the rates for three sites north of the Motagua Fault (indicated by the black
 1023 velocity arrows in Panel A). The error bars indicate the nominal 1-sigma rate uncertainties.
 1024
 1025



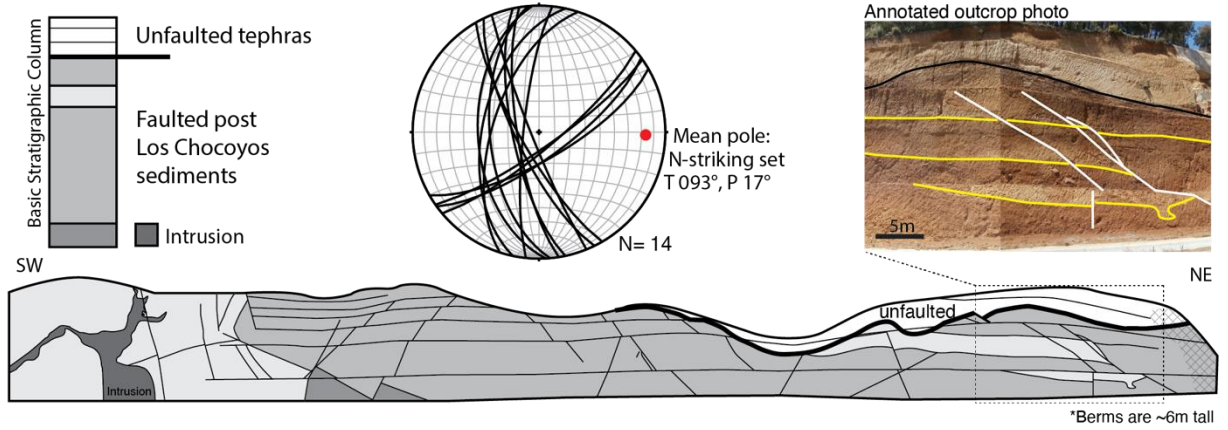
1026
 1027
 1028
 1029
 1030

Figure 4. Annotated DEM of the dashed box in Figure 1 with the locations of faulted outcrops. Each location is labeled along with major structures in western Guatemala.

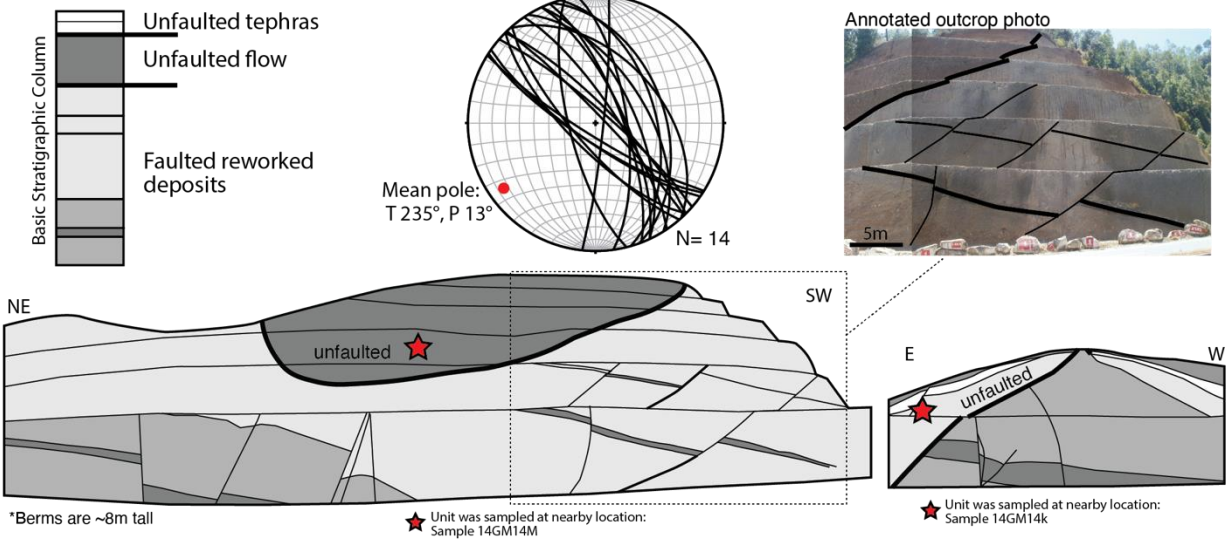


1031
 1032 Figure 5A. Annotated schematics of opposite facing roadcuts along the Santo Domingo Xenacoj
 1033 highway (Location 1). Mapview outcrop schematic shows the placement of the transects along
 1034 the roadcut, original lengths, and orientation and length of the final transect imposed onto the
 1035 orientation of maximum elongation. Stereonet displays the data from both transects.
 1036 Stratigraphic units and faults are identified on the annotated outcrops. Unconformities are
 1037 outlined with bolder lines, sections between unconformities are numbered 1 (oldest) to 7
 1038 (youngest) and correlated between outcrops. Yellow stars indicate transect endpoints and red
 1039 stars show locations where samples were collected.

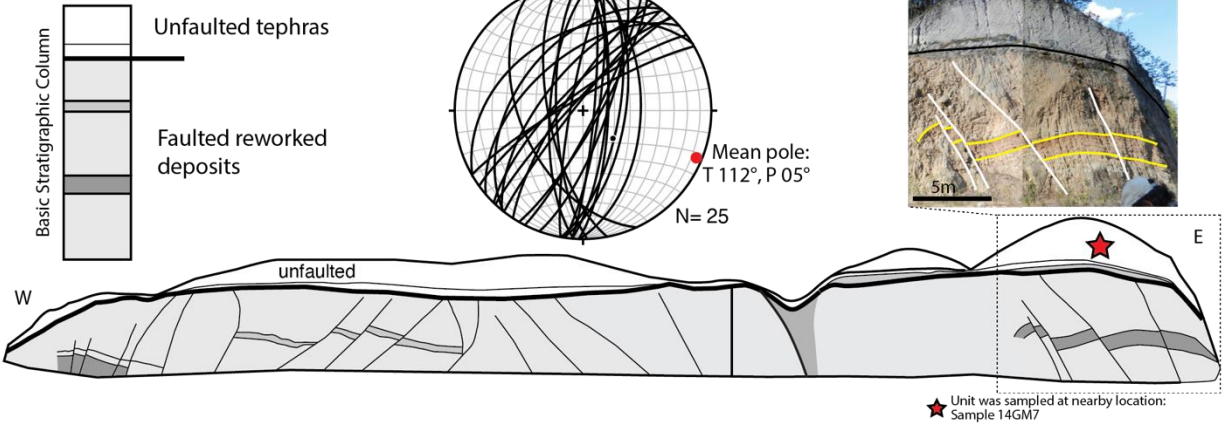
Tecpan Lat: 14.72 Long: -90.96



Nahuala Lat: 14.82 Long: -91.35



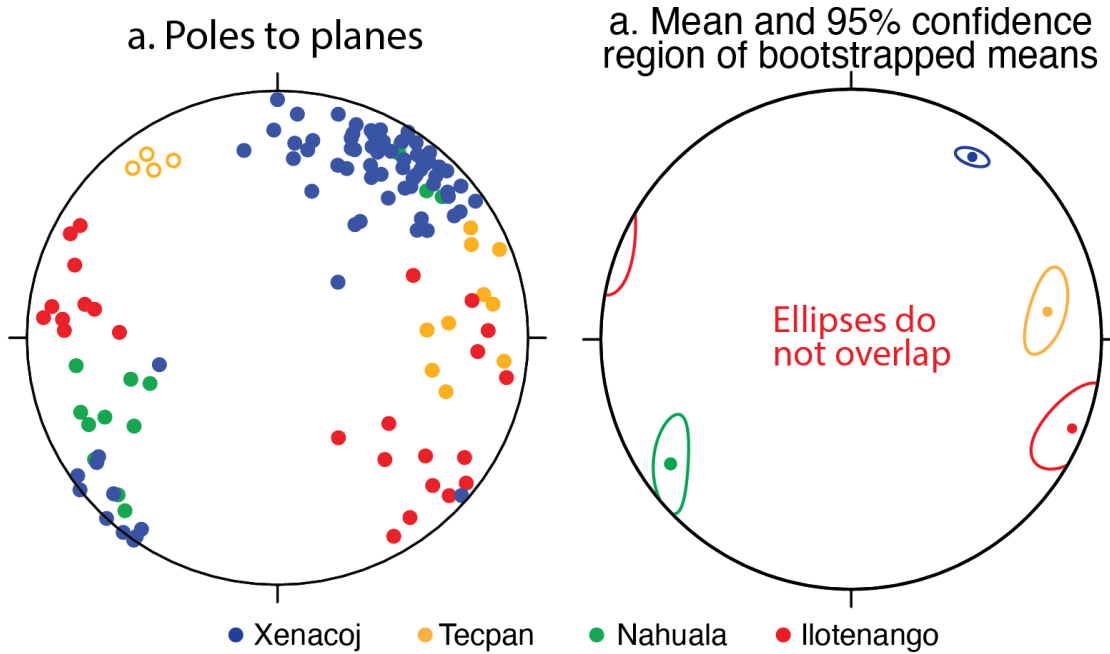
Ilotenango Lat: 15.04 Long: -91.23



1041
1042
1043

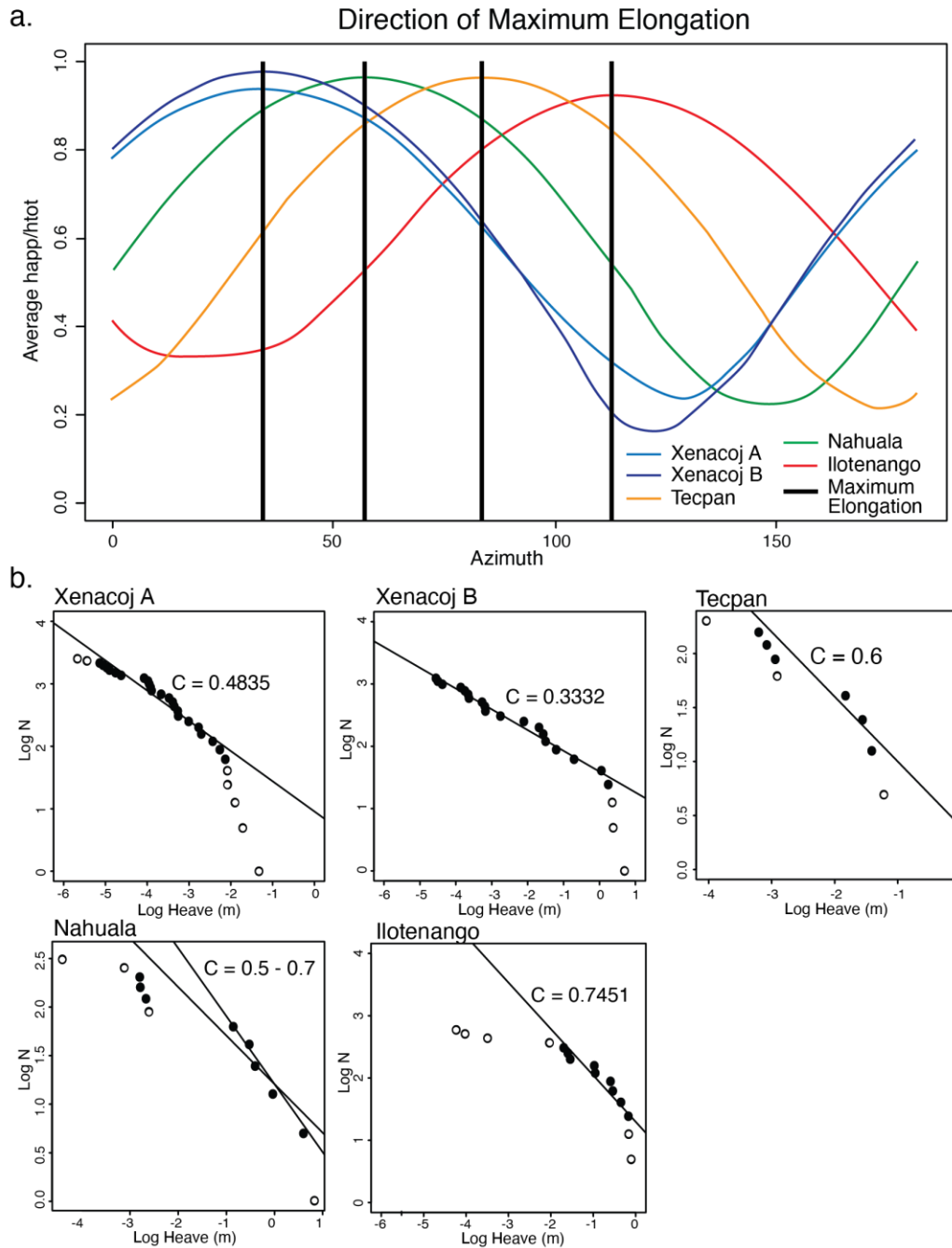
Figure 5B. Annotated outcrops and data from locations 2, 3, and 4. Similar labels to those in Figure 5A. In addition, an annotated outcrop photo is given for each location.

1044



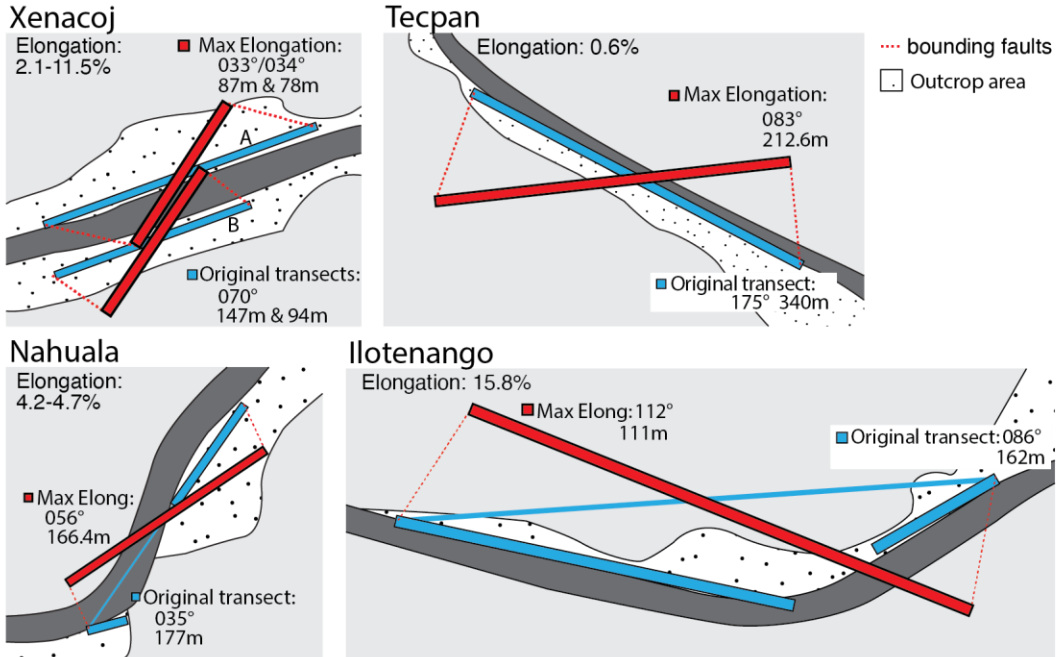
1045
1046
1047
1048
1049
1050
1051
1052

Figure 6. Fault data distribution, mean, and bootstrapped means. a. Poles of all fault data is displayed on a left lower-hemisphere stereonet and color-coded by location. The open dots for Tecpan represent the secondary fault set that was removed for the elongation estimations and for the bootstrapped means. b. The mean for each fault data set is projected, along with an ellipse that contains 95% of the bootstrapped mean. Ellipses for each data set do not overlap and indicate that the means are statistically different.



1053
 1054
 1055
 1056
 1057
 1058
 1059

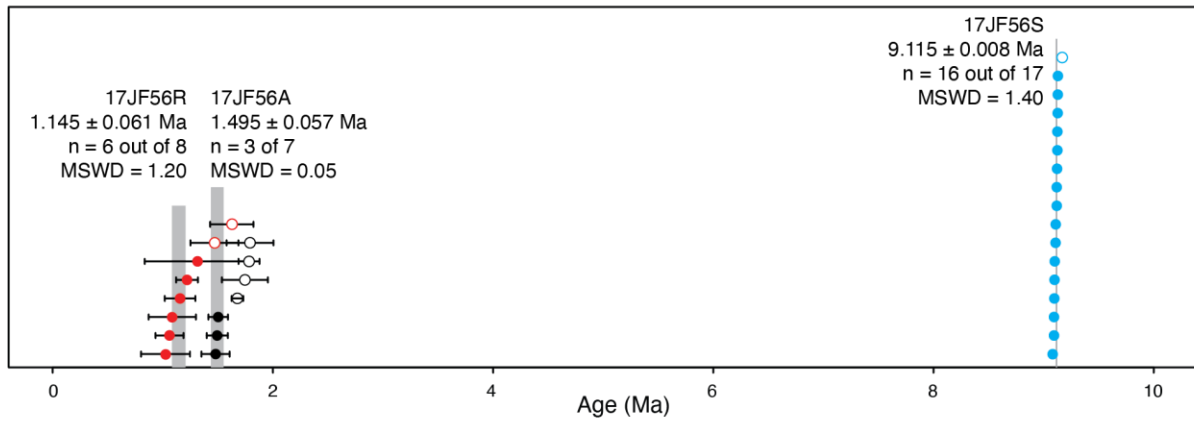
Figure 7. a. Plot displaying the relationship between apparent heave (happ) / total heave (htot) plot and orientation. The peak of each curve indicates the orientation of maximum elongation for each location. b. Frequency-displacement plots for fault data at each outcrop. Black data points indicate those used in the regression.



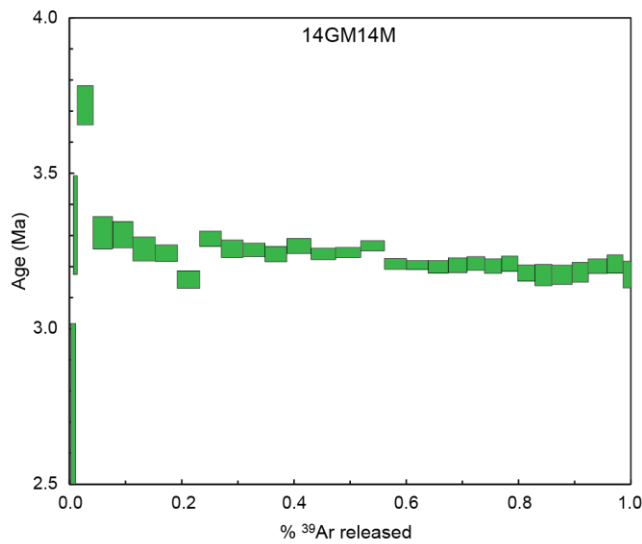
1060
 1061
 1062
 1063
 1064
 1065

Figure 8. Mapview schematics of each faulted outcrop. The length and orientation of the original faulted transects are displayed in blue and the transect projected onto the maximum elongation orientation are displayed in red. Red dashed lines are the orientation of the bounding faults.

a. Xenacoj

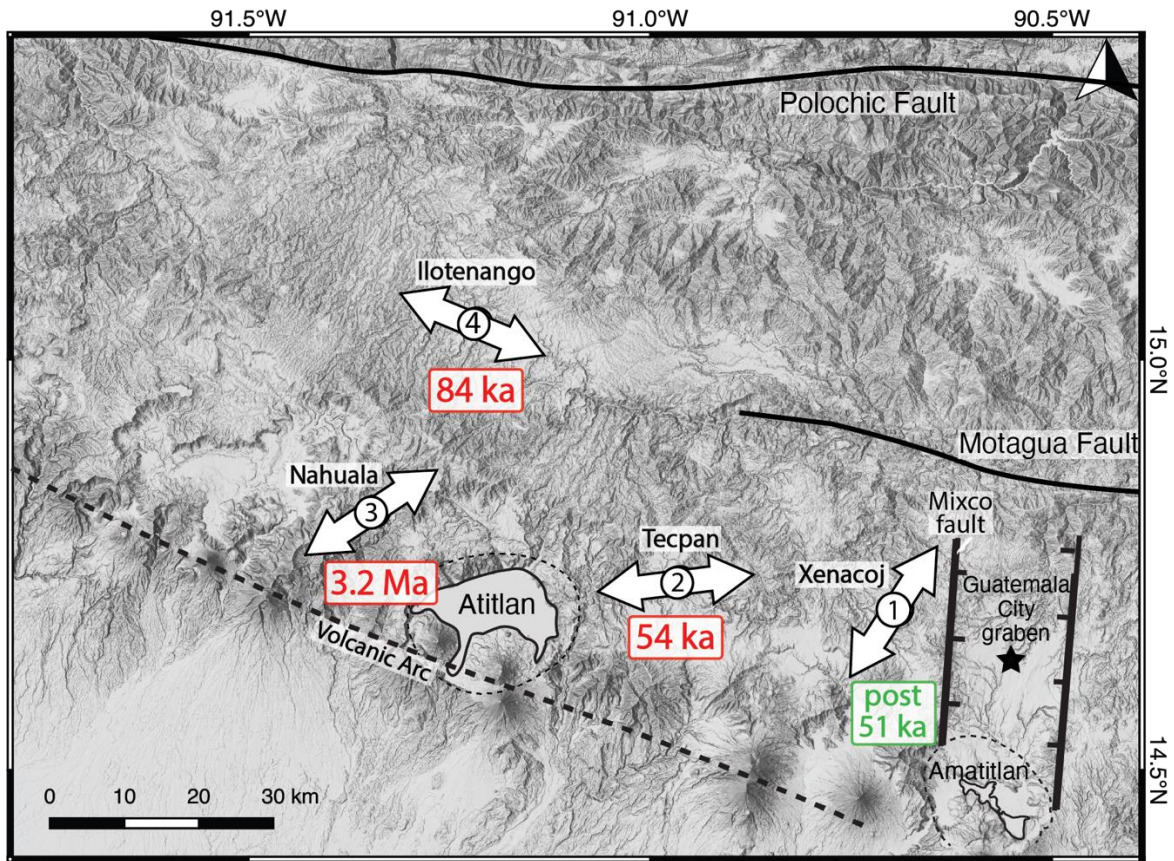


b. Nahuala



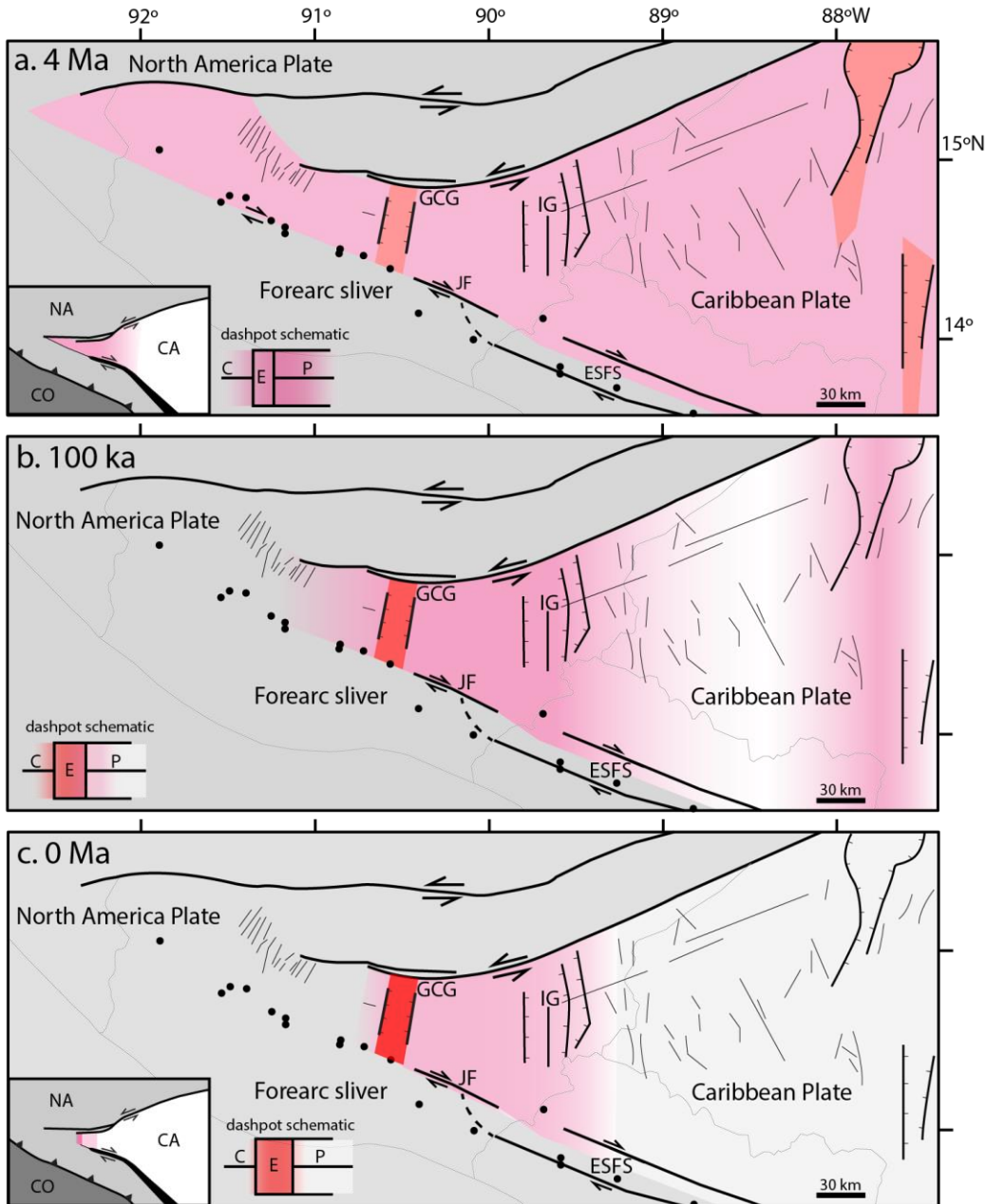
1066
 1067
 1068
 1069
 1070
 1071
 1072
 1073
 1074

Figure 9. $^{40}\text{Ar}/^{39}\text{Ar}$ data for four samples collected in western Guatemala. a. Rank order plots for the three tephra samples collected at Location 4 (17JF56R, 17JF56A, and 17JF56S). White dots are not included in weighted mean calculations. b. Age spectrum diagram for sample 14GM14M (Nahuala). The data do not yield a plateau. However, because most of the heating steps give ages between 3.3 and 3.2 Ma, we tentatively assume that this is a fair approximation for the age of this sample.



1075
 1076
 1077
 1078
 1079
 1080

Figure 10. Results from the minor fault analysis of western Guatemala. Arrows display the orientation of maximum elongation estimated for each location based on collected normal fault data. Below each location is the age of fault cessation. Star represents location of Guatemala City.



1081
 1082 Figure 11. Model of time progressive strain localization in the Caribbean wedge over the past 4
 1083 Ma. Color schematically indicates relative strain intensity. Abbreviations: NA- North America
 1084 plate; CA- Caribbean plate; CO- Cocos plate; GCG- Guatemala City graben; IG- Ipala graben;
 1085 JF- Jalpatagua fault; ESFS- El Salvador fault system; C- Dashpot cylinder; E- Extending region
 1086 of dashpot; P – Dashpot piston. a. 4 Ma (upper panel): Distributed ~east-west elongation took
 1087 place across major grabens and numerous minor faults from western Guatemala to western
 1088 Honduras. Inset maps show schematics of the larger tectonic system (left) and the system within
 1089 the dashpot analogy (right) during this time period with a broad extending region indicated with
 1090 pink. b. 100 ka (middle panel): Strain localized towards the Guatemala City and Ipala grabens,
 1091 ceasing movement on minor structures in western Guatemala, and in turn, transferring western
 1092 Guatemala to the North America plate and stabilizing the volcanic arc. Inset map shows the

1093 dashpot schematic of this time period with strain localizing within a narrower extending region
1094 as the upper panel, indicated with darker pink/red. c. 0 Ma (lower panel): East-west elongation
1095 is only observed across the Guatemala City graben and the Ipala graben, to a lesser extent.
1096 Deformation on minor structures has ceased. The Guatemala City graben is the western
1097 boundary between the North America and Caribbean plates. Inset maps show the schematics of
1098 the larger tectonic system (left) and the system viewed within the dashpot analogy (right) with
1099 strain localized within a bounded extending zone almost entirely between the cylinder and
1100 piston.